



ENLACE-ACI
MONTERREY, NUEVO LEÓN, MÉXICO

Synthetic macro fiber reinforced concrete

25th September 2025

Dr Peter Karoly Juhasz

INTRODUCTION OF JKP STATIC



Dr Peter Karoly JUHASZ

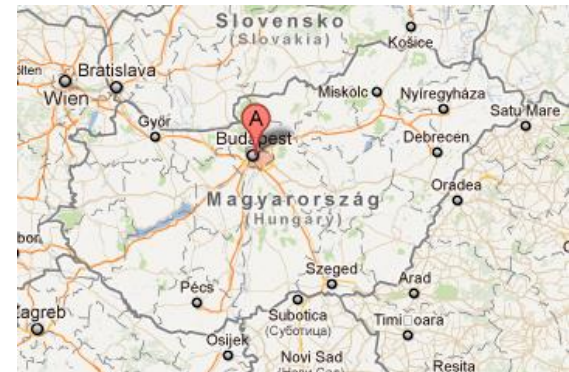
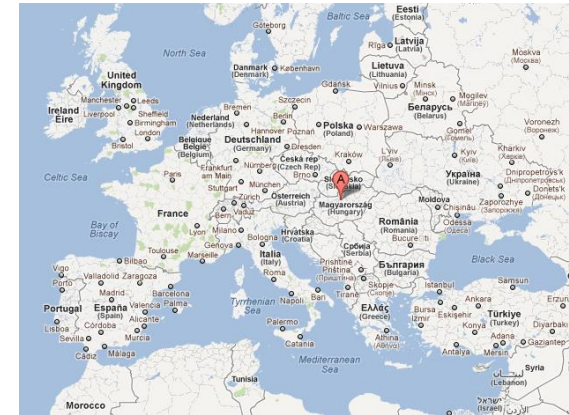
Structural engineer MSc PhD

Judit NAGY

Structural engineer BSc
Finite Element Analysis

Timea TUZA

Structural engineer MSc
Head of Laboratory



INTRODUCTION OF JKP STATIC

Dr Peter Karoly JUHASZ

Structural engineer MSc PhD

PhD specialization: fiber reinforced concrete

Positions

- Chief engineer at JKP STATIC
- Assistant professor at Budapest University of Technology

Past role

- Vice tutor Tongji University, Shanghai (2013)

Key contribution

- Modified Fracture Energy Method
 - Integrated into ATENA software
 - Referenced in ITAtech guideline
- Member of fib WP2.4.1 - Modelling of Fibre Reinforced Concrete Structures

Highlighted publications

- A Proposed Evaluation Method for Three-Point Beam Tests of Fiber-Reinforced Concrete (ASTM)
- Numerical and experimental investigation on synthetic macrofiber-reinforced concrete manhole exposed to railway loads (Elsevier)
- Improved evaluation of fiber reinforced concrete beam tests using an analytical model of fiber distribution and fracture cross-section location (Elsevier)



Table of contents

A. Fiber reinforced concrete – back to basics

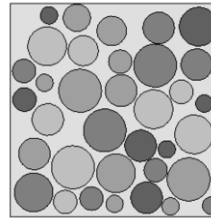
B. Calculation methods

C. Applications and case studies

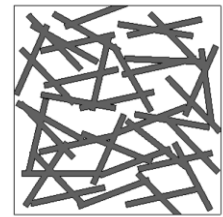
A. Fiber reinforced concrete – back to basics

A1. Introduction

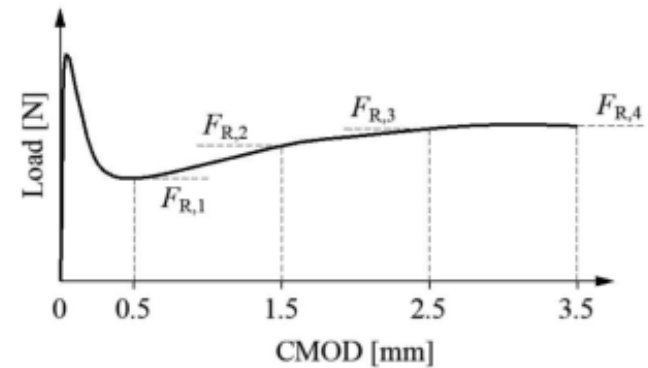
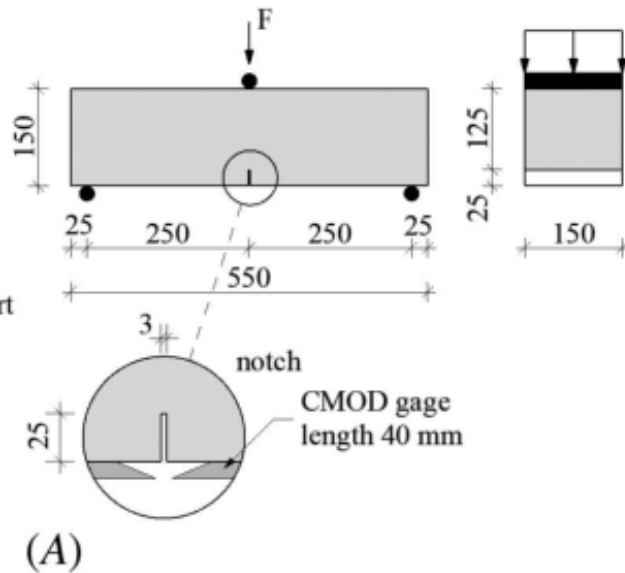
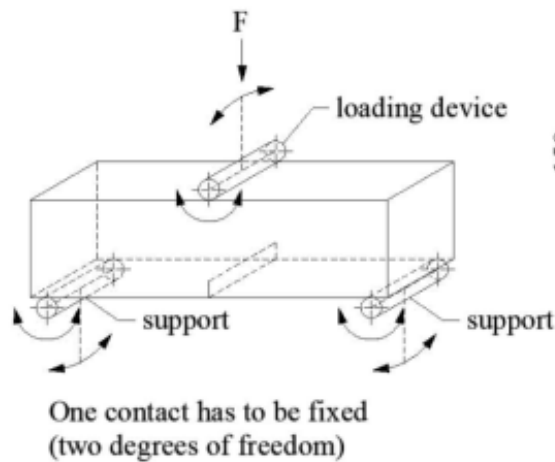
Concrete (matrix) + Fiber



+



Testing FRC

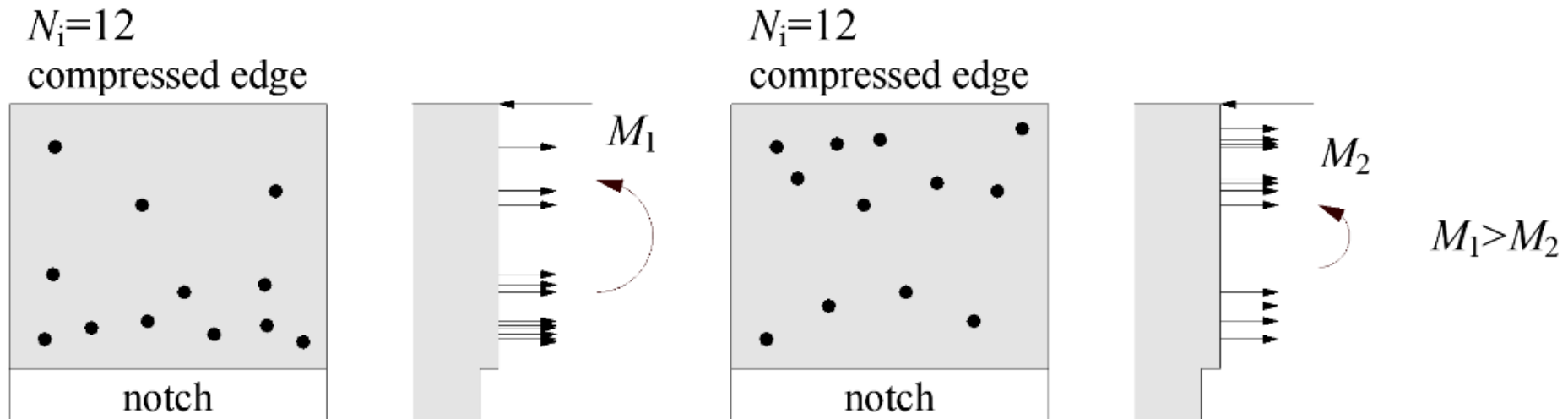


A2. Characterization of the cross-sectional distribution of fibers

A2.1. Fiber-moment

Fiber-moment

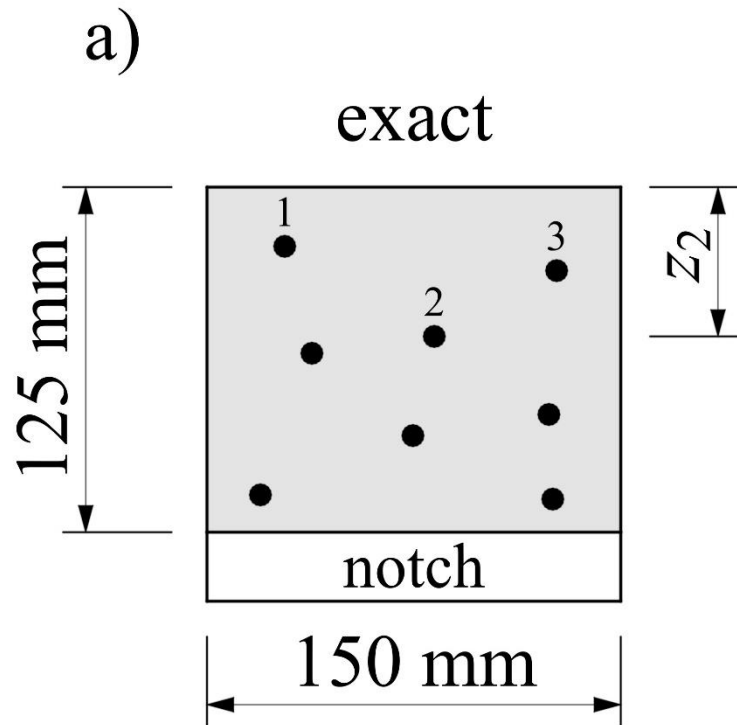
- a parameter to measure the location of the fibers on the cross section
- not used in the industry
- why is it useful?



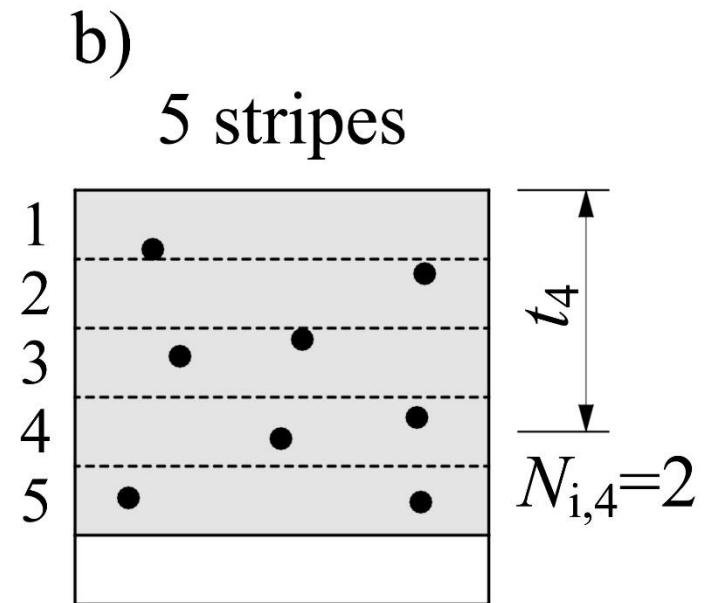
A2. Characterization of the cross-sectional distribution of fibers

A2.1. Fiber-moment

Measure fiber-moment



$$S_{f,\text{test}} = \sum_{s=1}^{N_i} z_s N_{i,s}$$

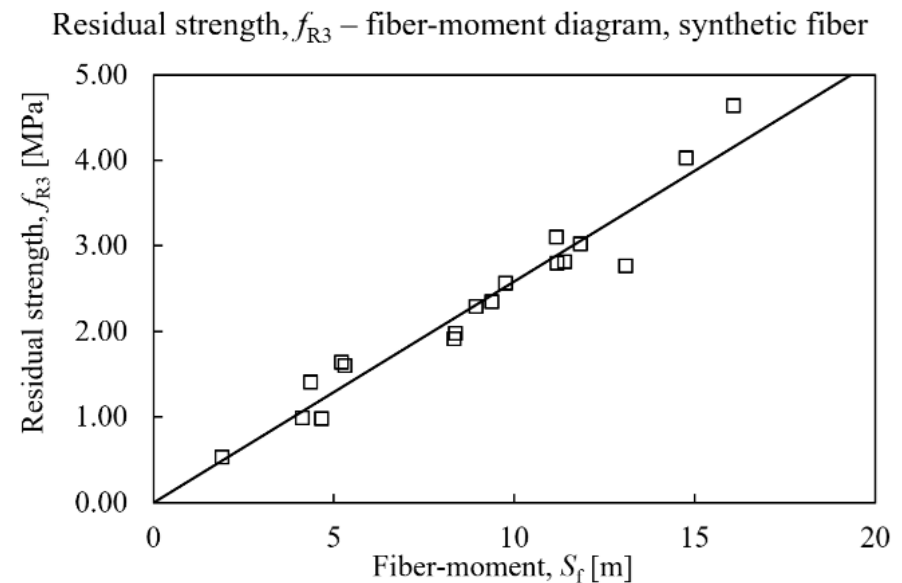
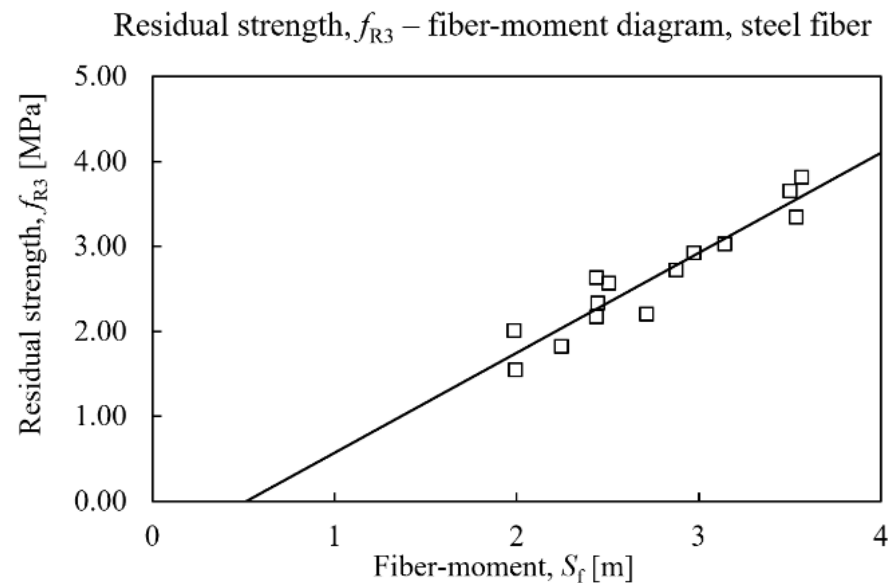


$$S_{f,\text{test}} = \sum_{j=1}^5 t_j N_{i,j}$$

A2. Characterization of the cross-sectional distribution of fibers

A2.1. Fiber-moment

Fiber-moment and residual strength

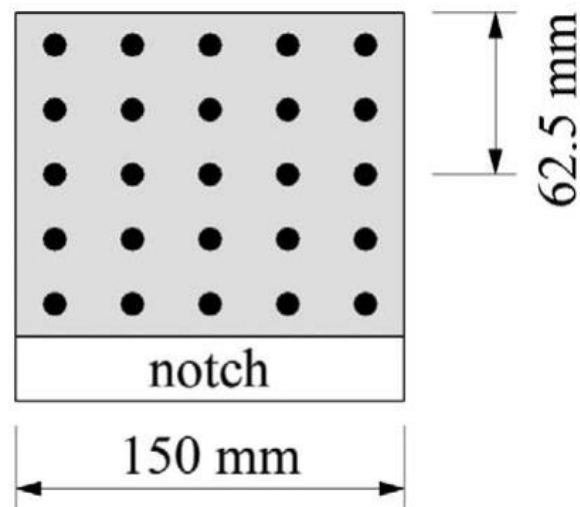


correlation coefficient $\delta > 0.9$

A2. Characterization of the cross-sectional distribution of fibers

A2.1. Fiber-moment

Ideal fiber-moment



$$S_{f,ideal} = N_i \frac{h}{2}$$

A2. Characterization of the cross-sectional distribution of fibers

A2.2. Fiber distribution

Clark-Evans (CE) aggregation index
nearest neighbour index

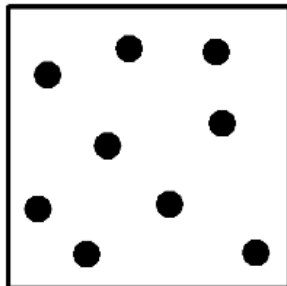
$$R = \frac{r_A}{r_E}$$

Hopkins-Skellam (HS) aggregation index

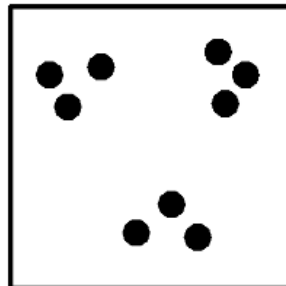
$$HS = \frac{\sum_i P_i^2}{\sum_i I_i^2}$$

a) random b) clustering and c) uniform

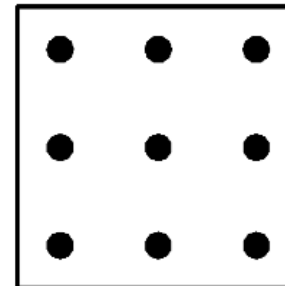
$R=1$
 $HS=1$



$R<1$
 $HS<1$

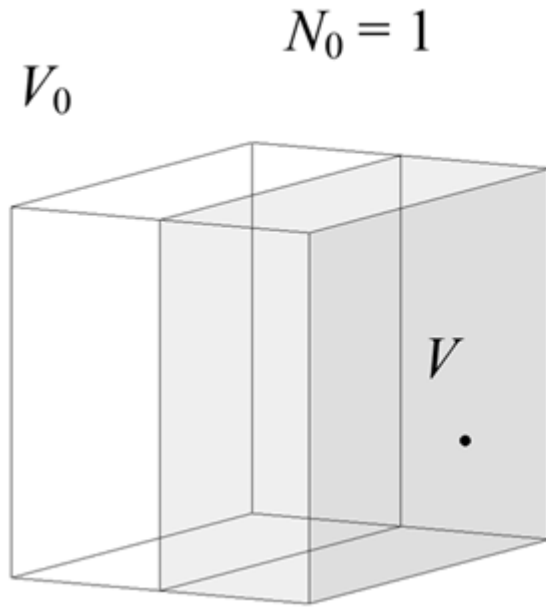


$R>1$
 $HS>1$

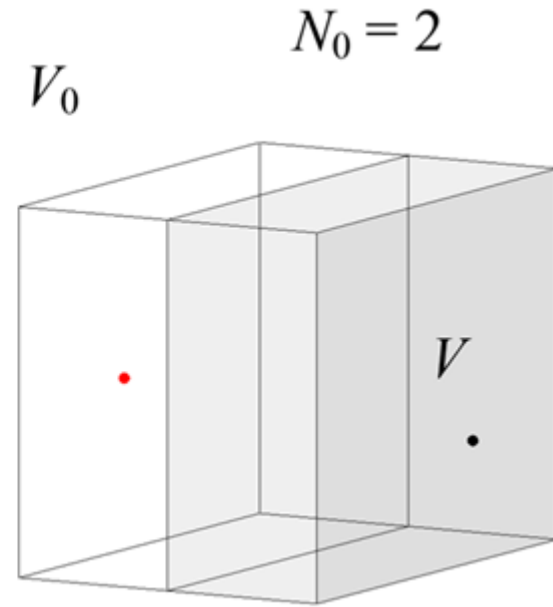


A3. Mixing modell

A3.1. Distribution of fibers in the matrix



$$P_1 = \frac{V}{V_0}$$



hypergeometric distribution \rightarrow large population
 \rightarrow binomial distribution

$$P_{1,n} = \binom{N_0}{n} P_1^n (1 - P_1)^{N_0 - n}$$

$$P = 0.5$$

$$N_0 = 2$$

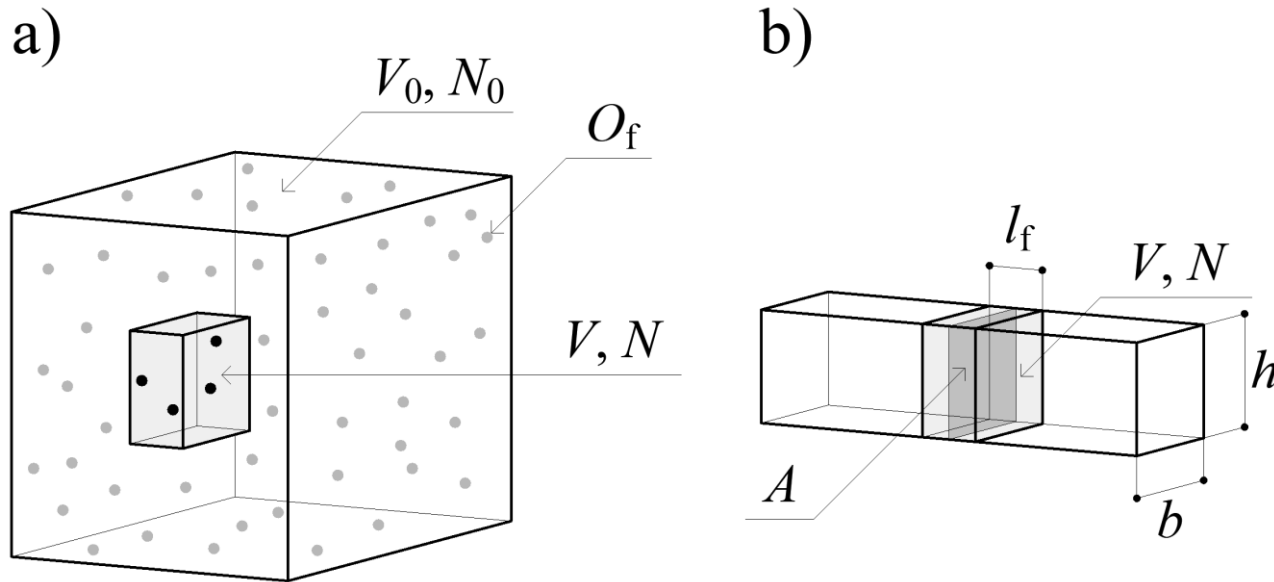
$$n = 0 \rightarrow 0.25$$

$$n = 1 \rightarrow 0.5$$

$$n = 2 \rightarrow 0.25$$

A3. Mixing modell

A3.1. Distribution of fibers in the matrix



$$m_1 = N_1 = P_1 N_0 = N_d V$$

$$\sigma_1 = \sqrt{N_0 P_1 (1 - P_1)}$$

$$CV = \frac{\sigma_1}{N_1} = \frac{1}{\sqrt{N_0}} \sqrt{\frac{V_0}{V} - 1}$$

Mean value

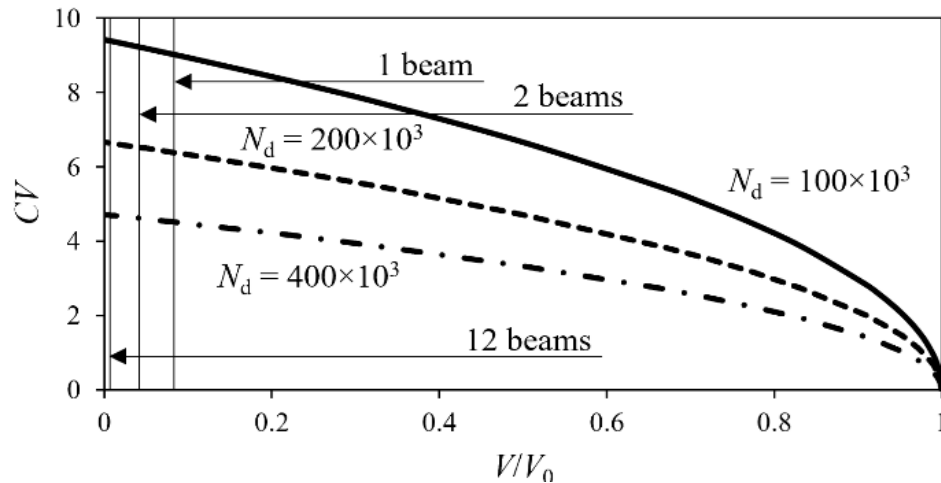
Standard deviation

Coefficient of variation

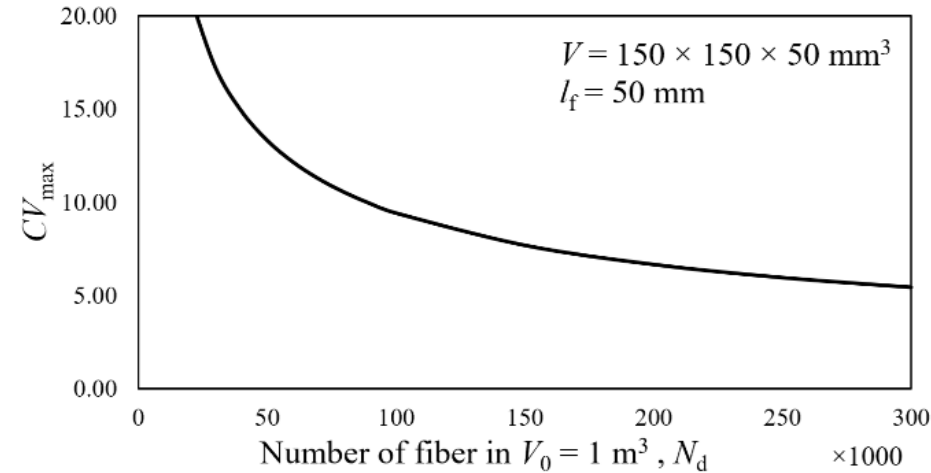
A3. Mixing modell

A3.1. Distribution of fibers in the matrix

Coefficient of variations of number of fibers in V



Correlation of dosage of fiber, N_d and CV_{\max}



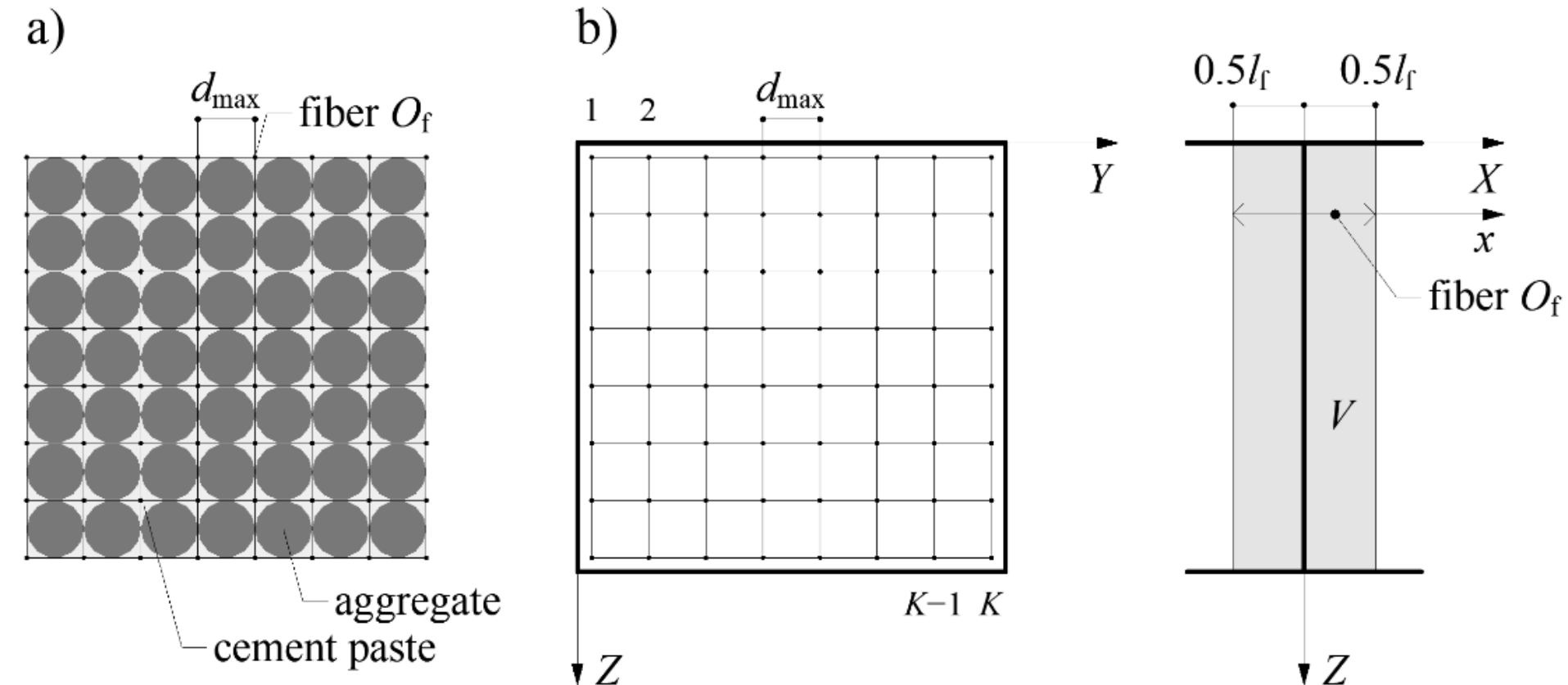
$$CV_{\max} = \lim_{V_0 \rightarrow \infty} \frac{1}{\sqrt{N_d V_0}} \sqrt{\frac{V_0}{V} - 1} = \frac{1}{\sqrt{N_d V}}$$

$$\sigma_{1,\max} = CV_{\max} N_1 = \sqrt{N_d V}$$

$$N \in \left[N_1 - 1.645 \sigma_{1,\max}; N_1 + 1.645 \sigma_{1,\max} \right]$$

A3. Mixing modell

A3.2. Position of the fibers in the matrix

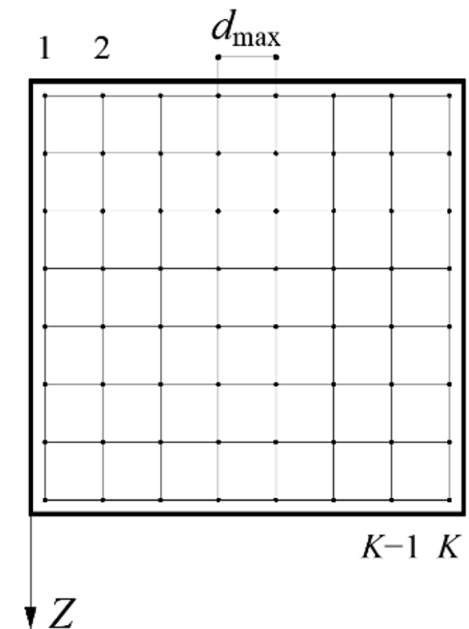


A3. Mixing modell

A3.2. Position of the fibers in the matrix

In a volume V , N fibers are randomly distributed across K lattice points.

- If $N < K$, the fibers are placed randomly at the lattice points, ensuring that no lattice point contains more than one fiber.
- If $N = K$, each lattice point will contain exactly one fiber.
- If $N > K$, the first K fibers are placed such that each lattice point contains one fiber, and the remaining $N - K$ fibers are randomly distributed among the lattice points.
- If $N - K > 2K$ two fibers are initially placed at each lattice point, with the remaining $N - 2K$ fibers being randomly distributed across the lattice points. This logic is iteratively applied as necessary.



A3. Mixing modell

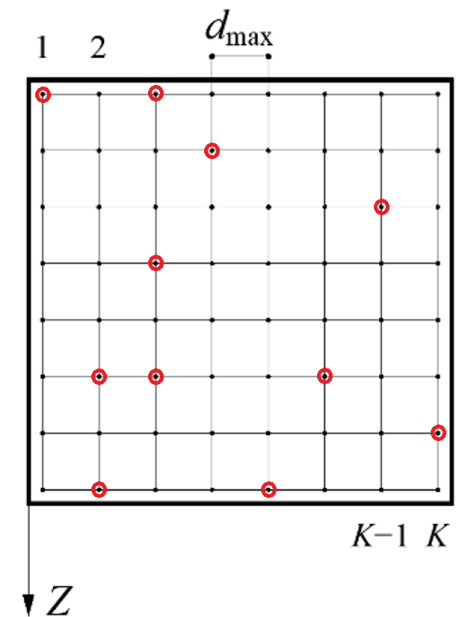
A3.2. Position of the fibers in the matrix

Based on the model, the distribution of fibers is assumed to be uniform, which does not account for potential clustering observed in real experiments.

To incorporate clustering, the **placement of fibers can be restricted at certain randomly selected lattice points**.

Let $\gamma = K_e/K$, where γ is the clustering factor, K_e denotes the number of excluded lattice points and K represents the total number of lattice points.

In this case, clustering is enforced during fiber placement, even when the number of fibers is smaller than the number of lattice points.



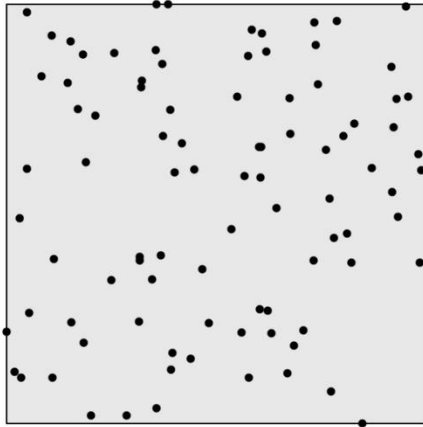
A3. Mixing modell

A3.2. Position of the fibers in the matrix

$$d_{\max} = 8 \text{ mm}$$

$$\gamma = 0$$

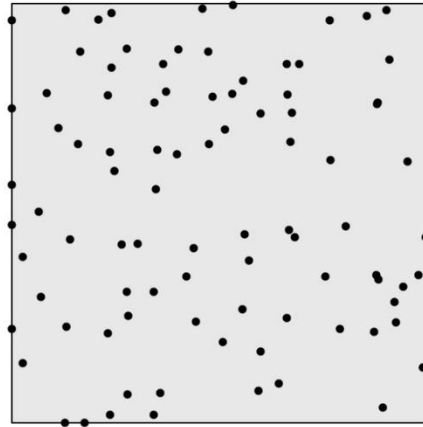
$$N_i = 92$$



$$d_{\max} = 16 \text{ mm}$$

$$\gamma = 0$$

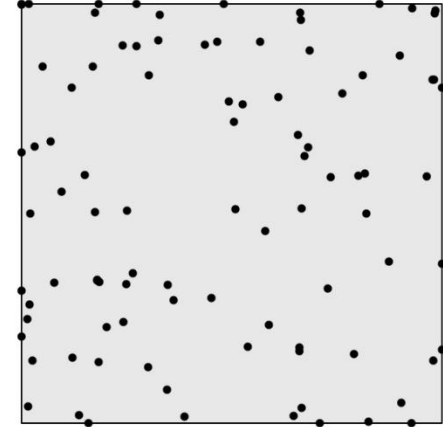
$$N_i = 96$$



$$d_{\max} = 24 \text{ mm}$$

$$\gamma = 0$$

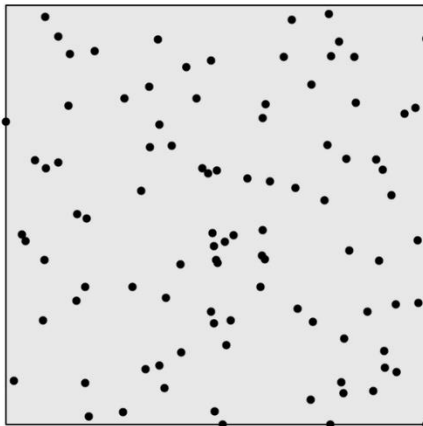
$$N_i = 94$$



$$d_{\max} = 8 \text{ mm}$$

$$\gamma = 0.5$$

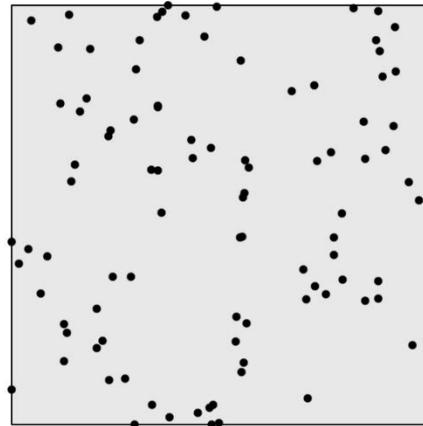
$$N_i = 97$$



$$d_{\max} = 16 \text{ mm}$$

$$\gamma = 0.5$$

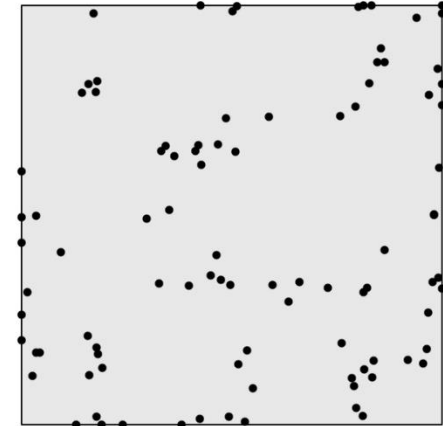
$$N_i = 95$$



$$d_{\max} = 24 \text{ mm}$$

$$\gamma = 0.5$$

$$N_i = 94$$



A3. Mixing modell

A3.3. Cross-sectional intersection of fibers

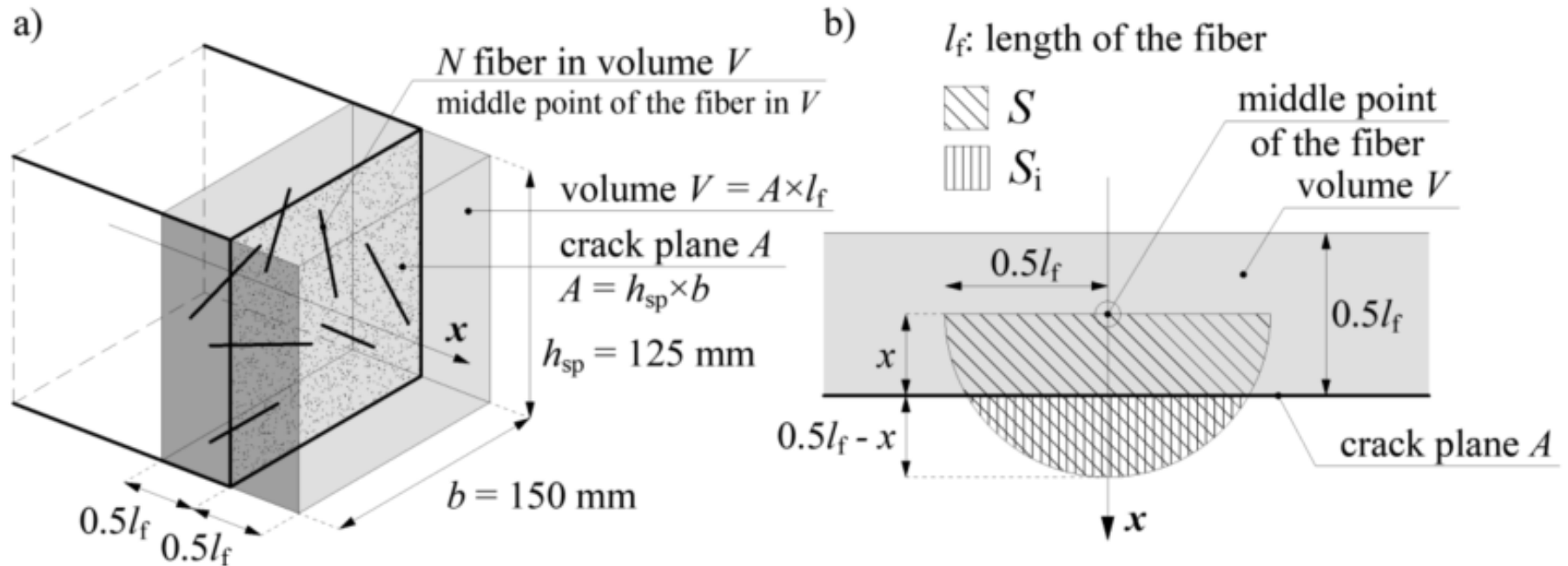


Figure 1: a) Crack plane A and volume V; b) geometric probability of intersection

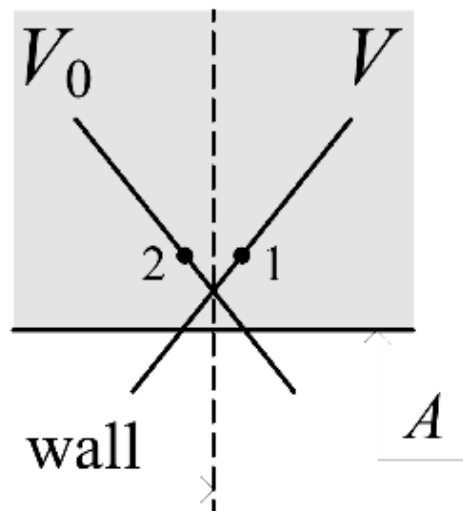
$$m_2 = N_2 = P_2 N_1 = 0.5 N_1 = 0.5 N_d V$$

$$\sigma_2 = \sqrt{N_2 P_2 (1 - P_2)} = \sqrt{0.25 N_2} = \sqrt{0.125 N_d V}$$

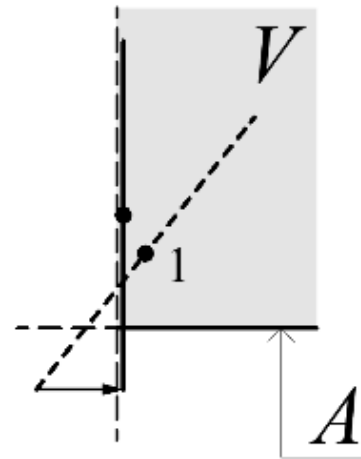
A3. Mixing modell

A3.4. Wall-effect

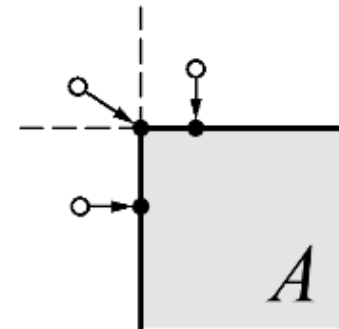
a)



b)



c)



A3. Mixing modell

A3.5. Model formulation

$$N_i = m_i = P_1 P_2 N_0 = 0.5 N_d V$$

$$\sigma_i = \sqrt{\sigma_1^2 + P_2^2 \sigma_1^2 + \sigma_2^2} = \sqrt{1.25\sigma_1^2 + \sigma_2^2} = \sqrt{1.25N_d V + 0.125N_d V} = \sqrt{1.375N_d V}$$

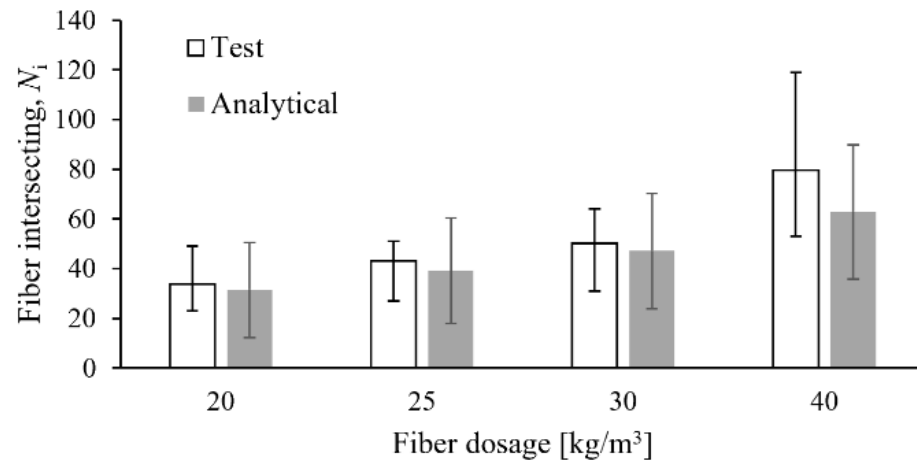
$$CV_i = \sqrt{5.5} \frac{1}{\sqrt{N_d V}}$$

$$\left[N_i - 1.645\sigma_i ; N_i + 1.645\sigma_i \right]$$

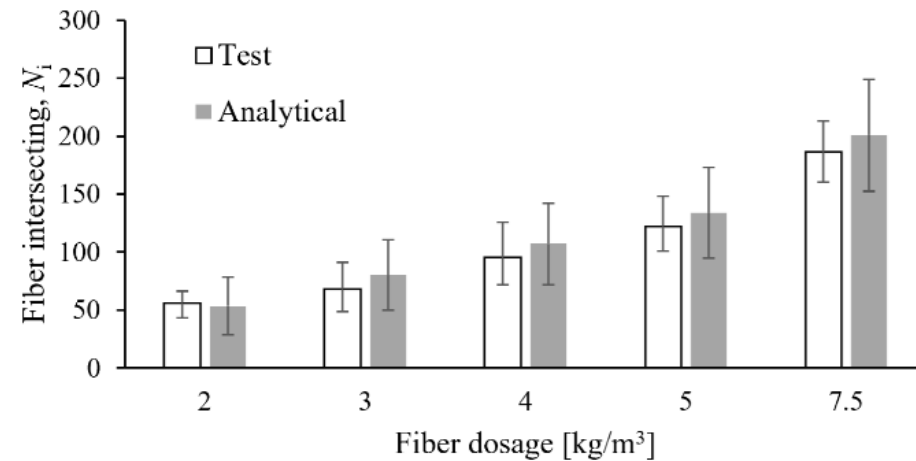
A4. Comparison of analytical and laboratory results

A4.1. Number of fibers intersecting the cross section

Steel fiber intersecting test and analytical

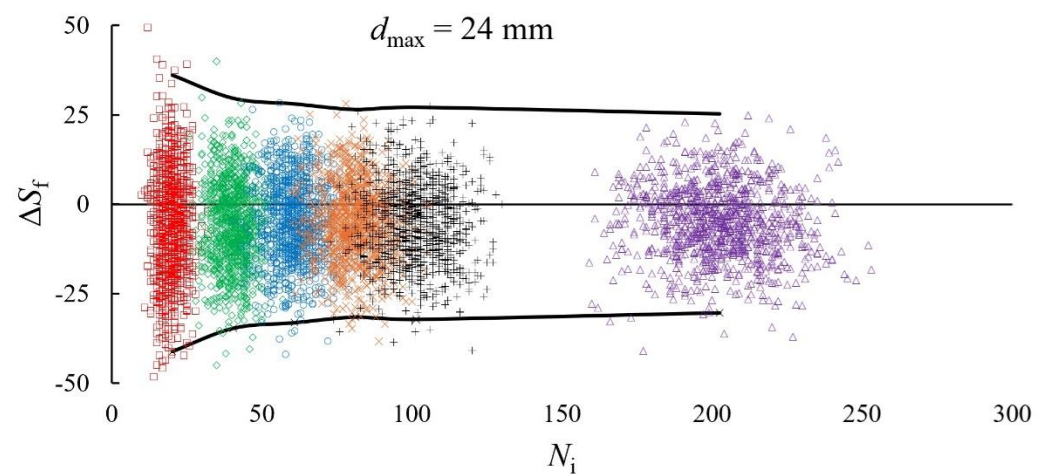
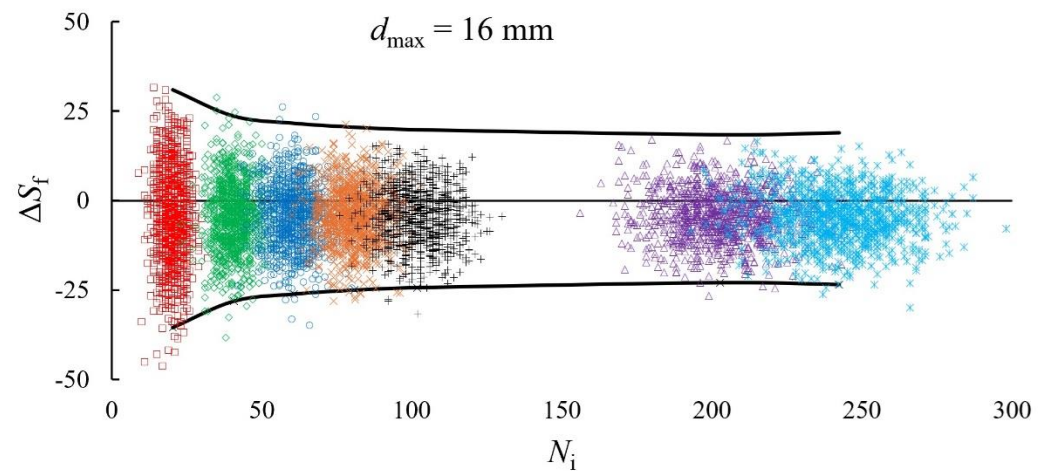
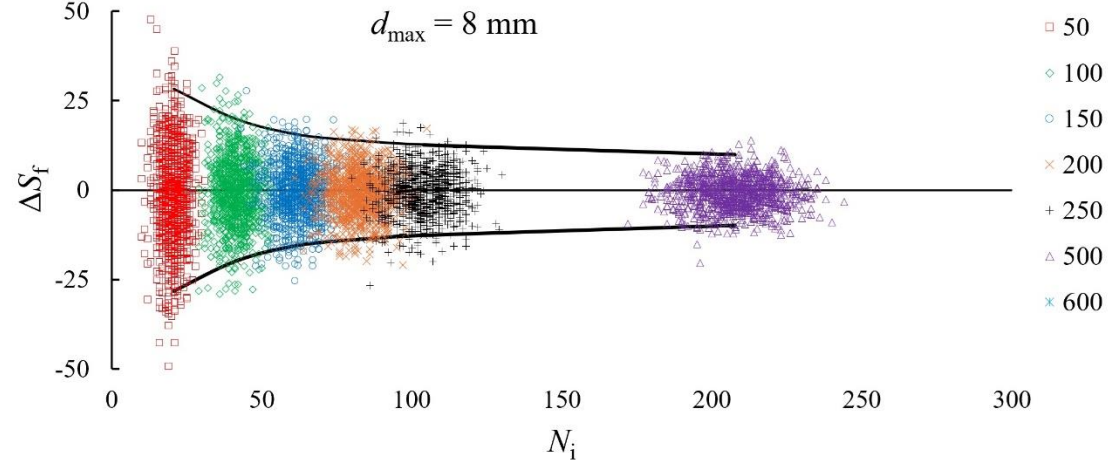


Synthetic fiber intersecting test and analytical



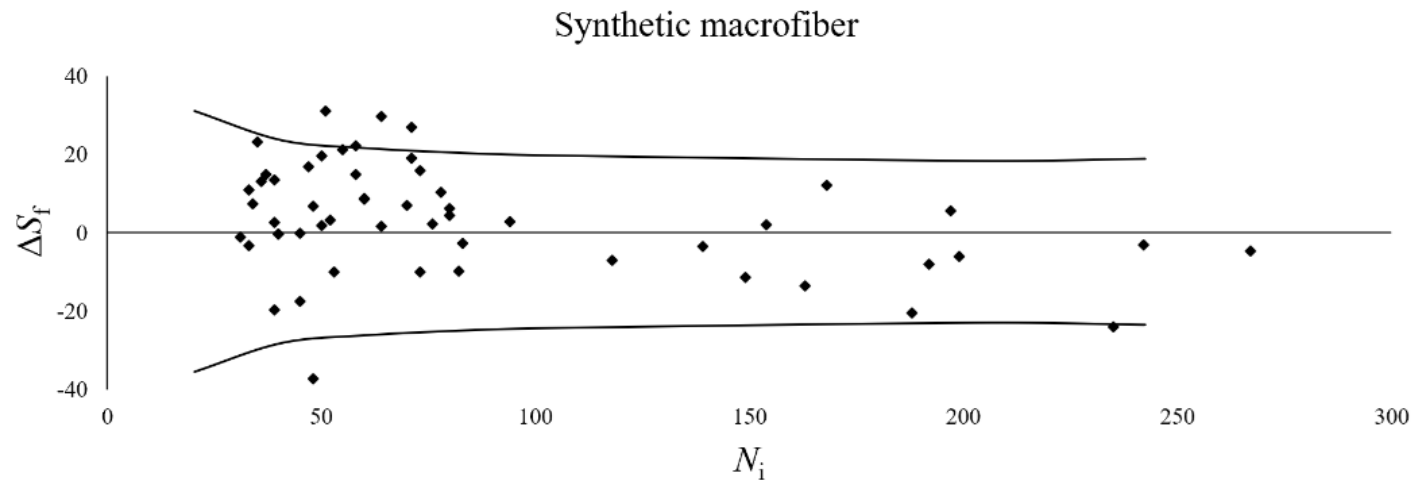
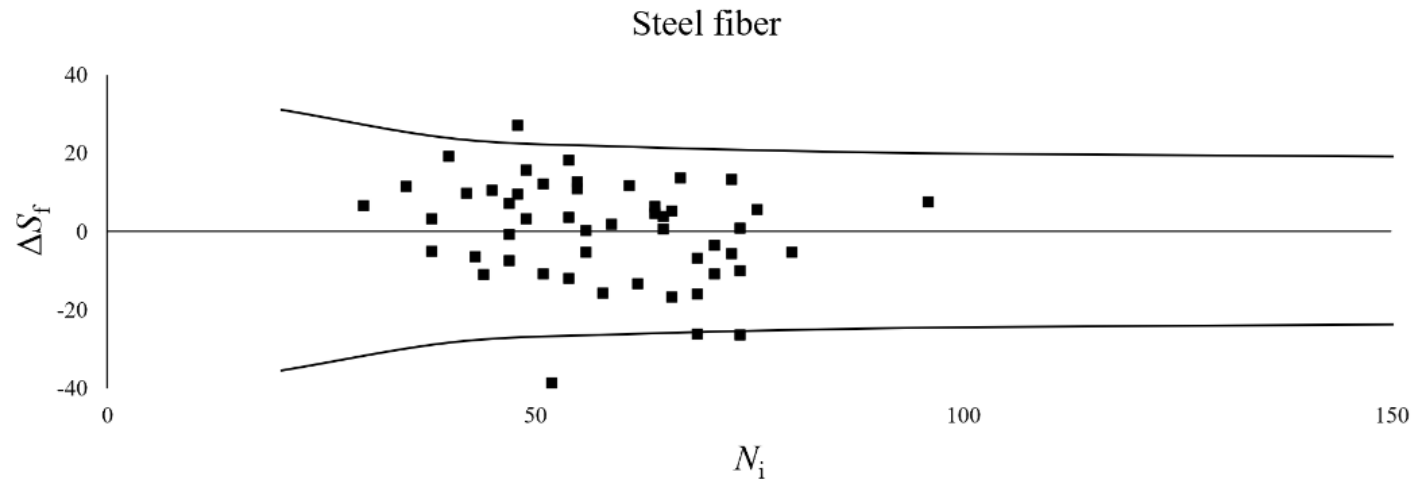
A4. Comparison of analytical and laboratory results

A4.2. Effect of number of fibers and aggregate size on the fiber-moment



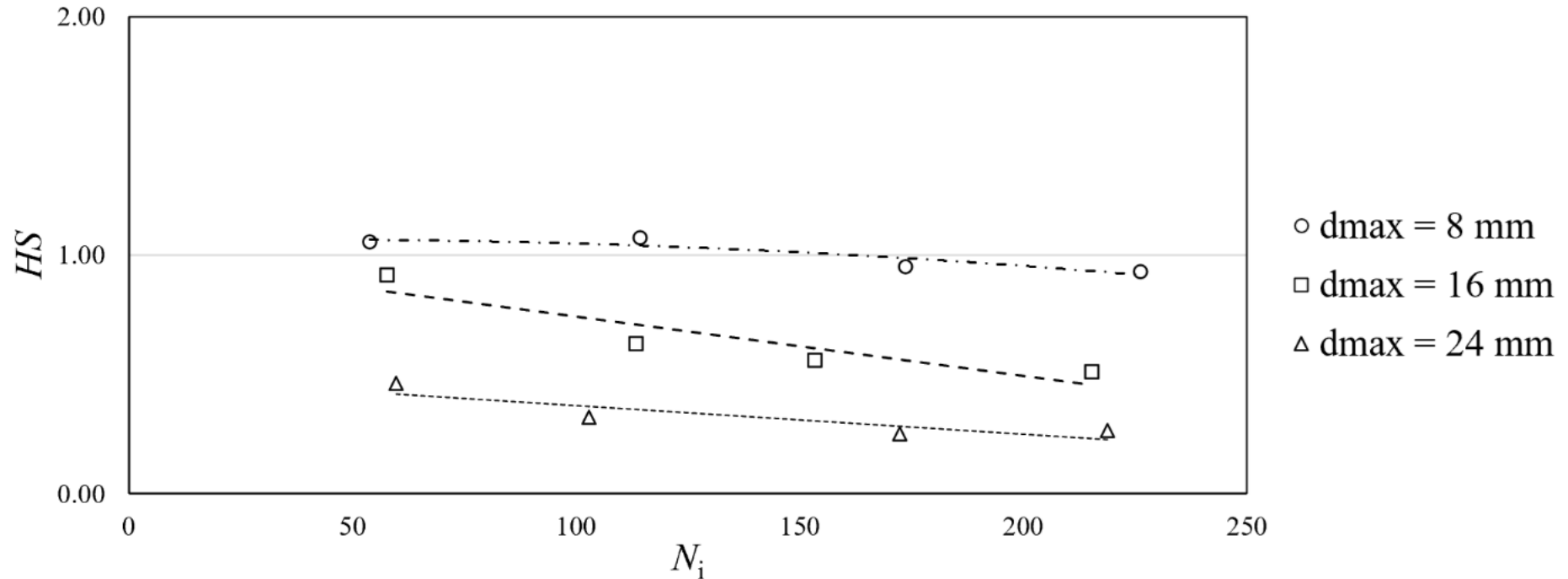
A4. Comparison of analytical and laboratory results

A4.2. Effect of number of fibers and aggregate size on the fiber-moment

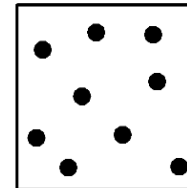


A4. Comparison of analytical and laboratory results

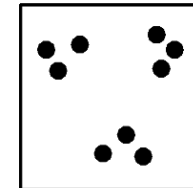
A4.3. Uniformity of intersection points on cross section



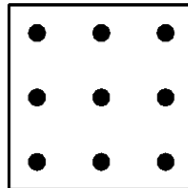
$R=1$
 $HS=1$



$R<1$
 $HS<1$

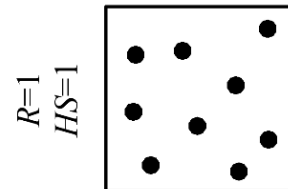
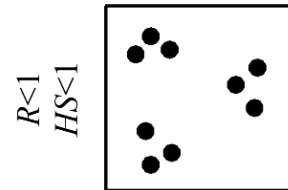
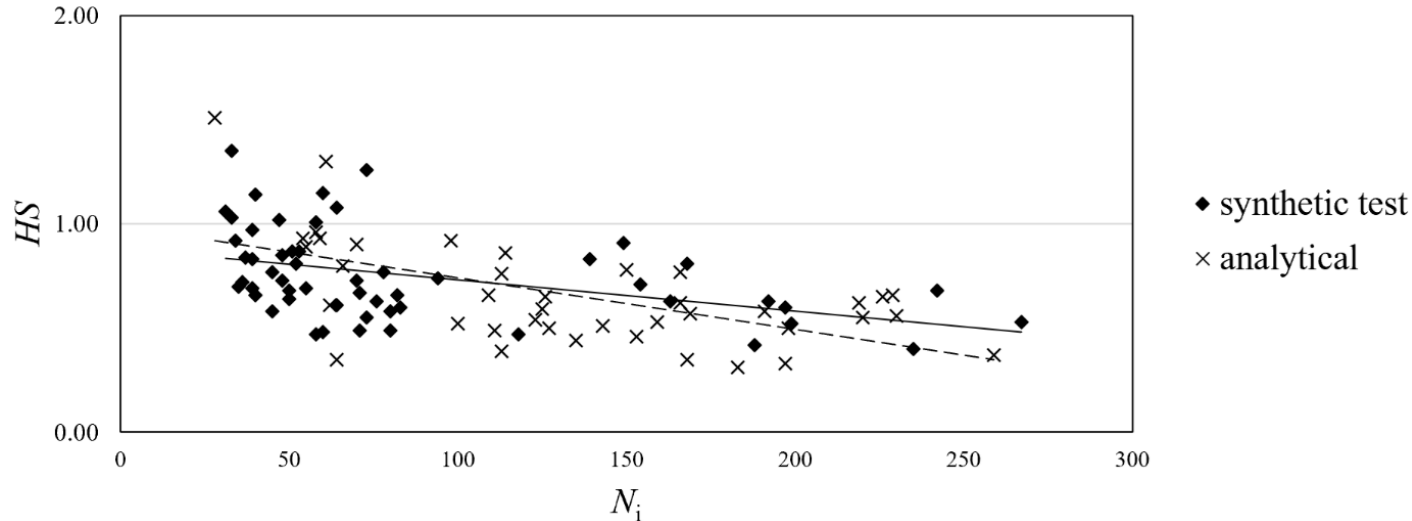
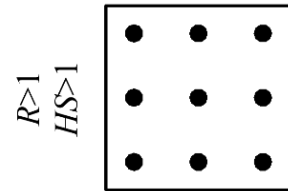
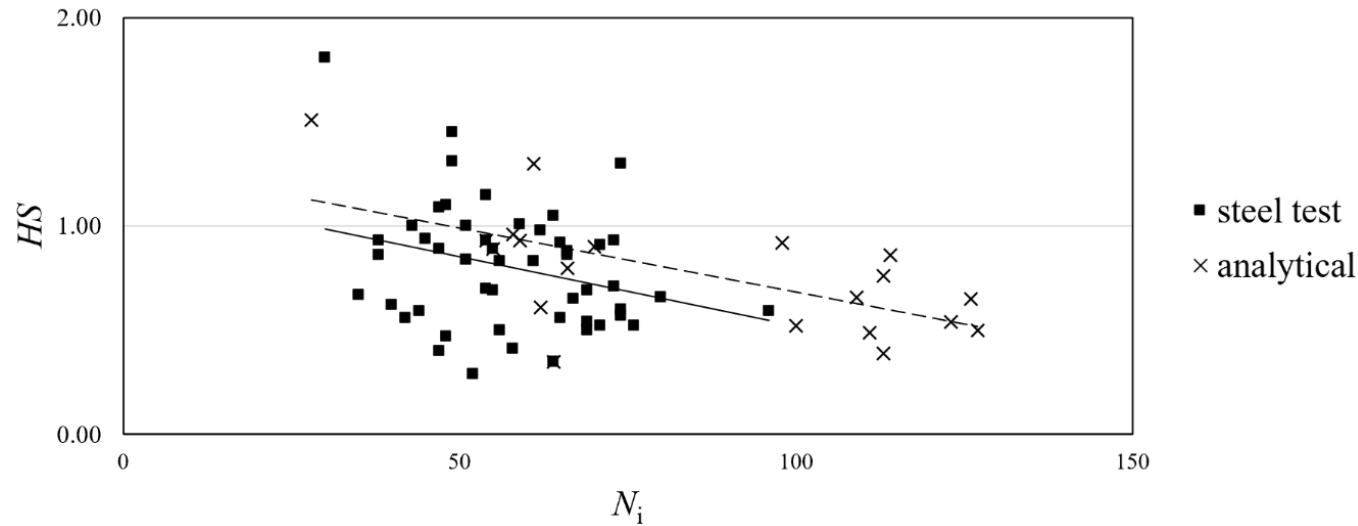


$R>1$
 $HS>1$



A4. Comparison of analytical and laboratory results

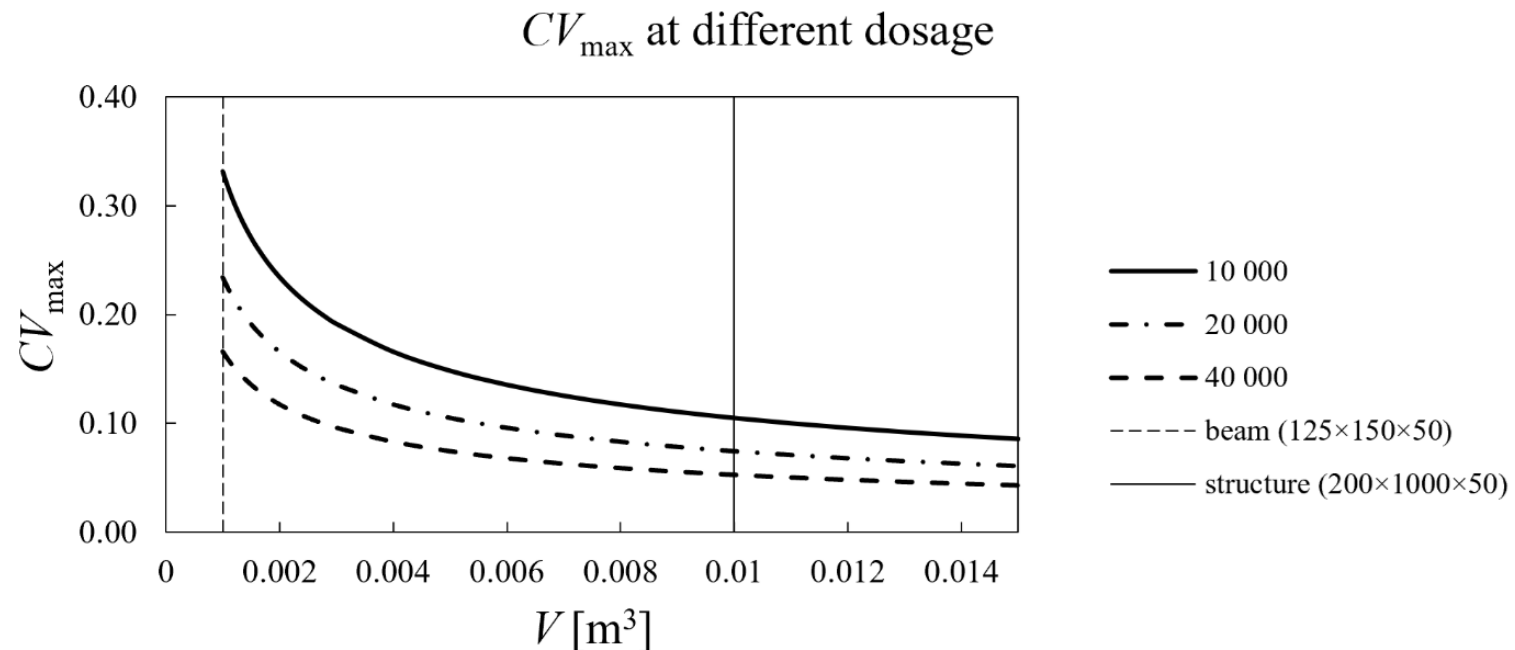
A4.3. Uniformity of intersection points on cross section



A5. Conclusion

A5.1. The effect of the number and variability of fibers intersecting the cross-section on the characteristic value

$$f_{R,i,k} = f_{R,i,m} (1 - 1.645 CV_i)$$



Standard beam section:

$$4 \text{ MPa} \times (1 - 1.645 \times 0.23) = 4 \text{ MPa} \times 0.62 = 2.48 \text{ MPa}$$

Typical structure section:

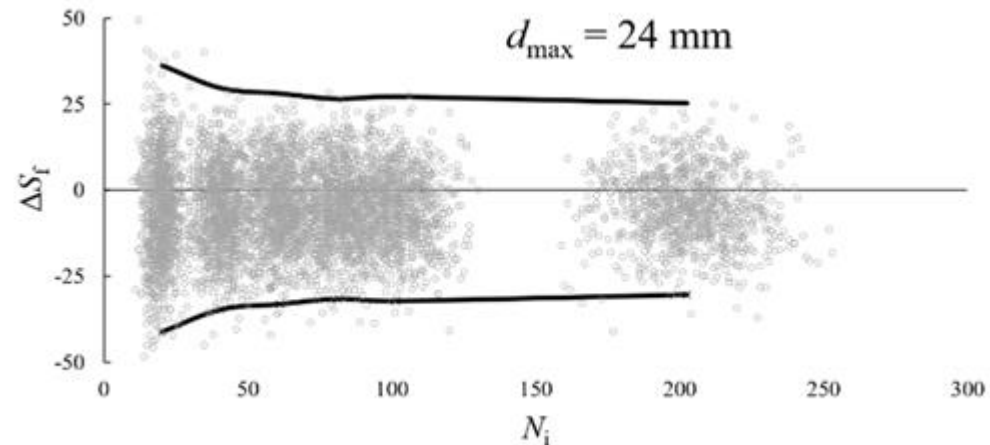
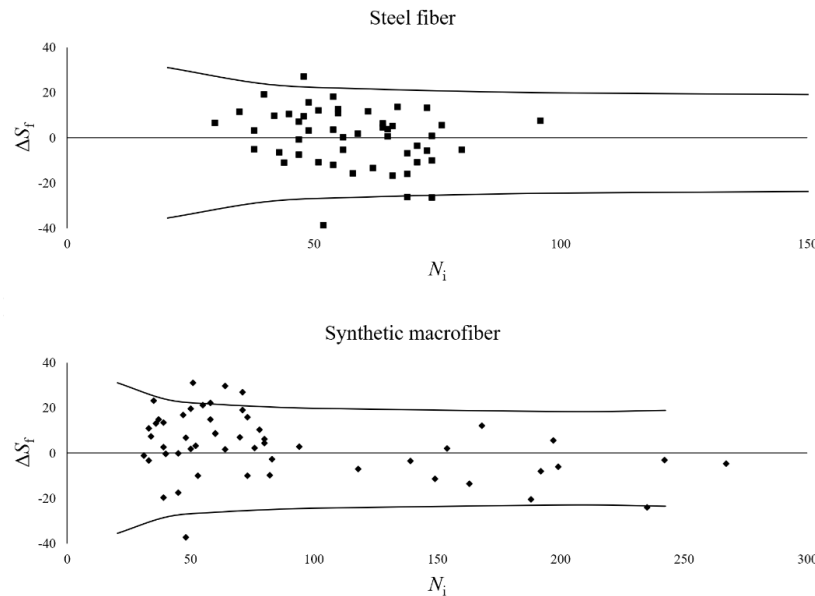
$$4 \text{ MPa} \times (1 - 1.645 \times 0.07) = 4 \text{ MPa} \times 0.88 = 3.53 \text{ MPa (+42\%)}$$

A5. Conclusion

A5.1. The effect of the number and variability of fibers intersecting the cross-section on the characteristic value

The effect of the fiber-moment

According to the current study, as a conservative approximation, a 25% deviation can be applied for beam cross-sections when $N > 50$



A5. Conclusion

A5.2. Clustering propensity

as the number of fibers increases, the likelihood of fibers clustering within the cross-section also increases

model provides a good approximation for both steel and synthetic macrofibers

according to the analytical model, clustering is less significant with smaller aggregate sizes compared to larger aggregate sizes

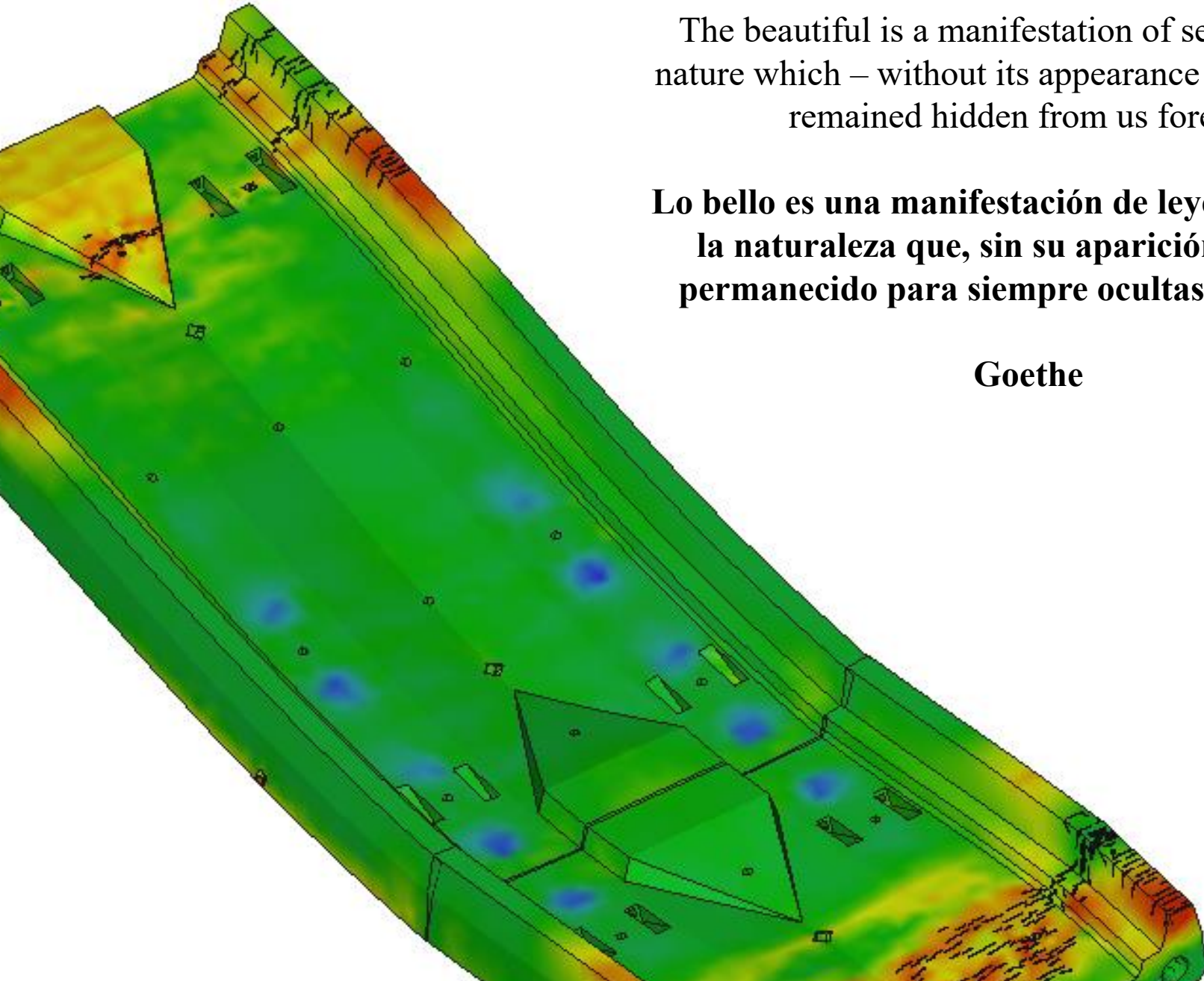
This study explores the influence of fiber distribution and orientation on the mechanical properties of FRC using an analytical mixing model supported by experimental validation. The findings highlight the critical role of fiber dosage, reference volume, and aggregate size in determining the number of fibers intersecting a cross-section and their clustering behavior. Clustering becomes more pronounced as the fiber dosage increases, with steel fibers showing greater clustering tendencies at lower dosages compared to synthetic macrofibers.

The **fiber-moment**, which depends on the spatial distribution of fibers, has a significantly affect on the load-bearing capacity of FRC bent beams. **Larger deviations from the ideal fiber-moment occur with fewer fibers and larger aggregate sizes.** A strong correlation between fiber-moment and residual strength underscores the importance of accounting for fiber positioning in evaluating FRC performance.

The analytical mixing model accurately predicts the number of fibers intersecting the cross-section, clustering behavior, and variability due to fiber location, orientation, and aggregate size. Experimental results validated these predictions, demonstrating the robustness of the model for standard-sized beams. By incorporating fiber-moment and distribution into characteristic value calculations, the proposed method reduces variability and improves the reliability of design parameters. For beam cross-sections with a fiber count greater than 50, a 25% deviation from the ideal fiber-moment is suggested as a conservative approach.

While the model enhances the accuracy of beam tests, its applicability to other structural configurations warrants further investigation. The effect of clustering and fiber distribution on residual strength remains an area for future study. This research offers a robust methodology that resolves critical limitations in current FRC testing standards, enabling more economical and reliable designs.

B. Calculation methods



The beautiful is a manifestation of secret laws of nature which – without its appearance – would have remained hidden from us forever.

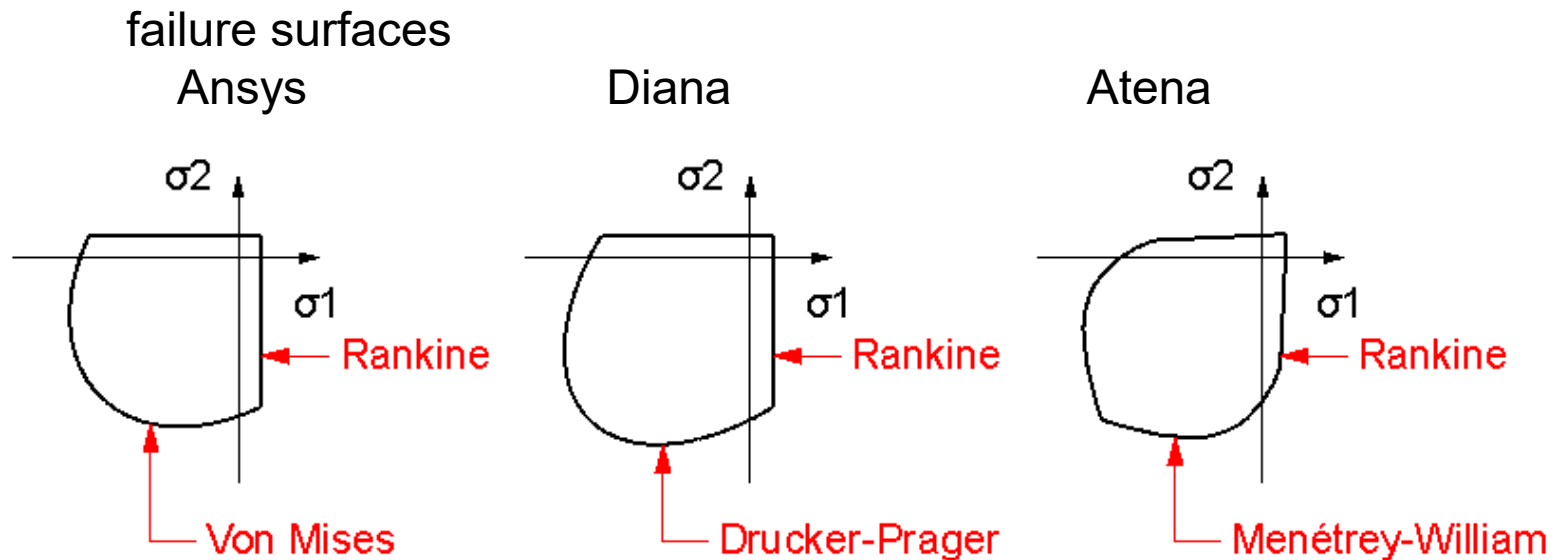
Lo bello es una manifestación de leyes secretas de la naturaleza que, sin su aparición, habrían permanecido para siempre ocultas a nosotros.

Goethe

B1. Material models

from linear elastic to concrete

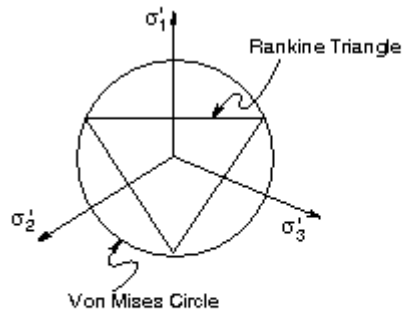
1) Different behaviour in compression or tension



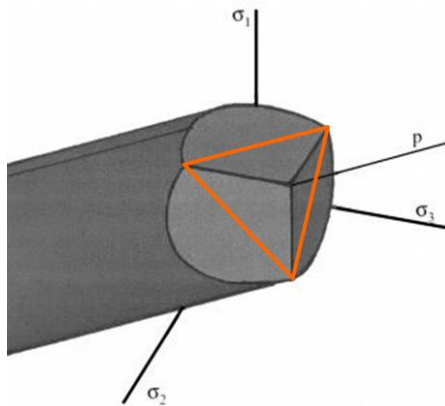
B1. Material models

from linear elastic to concrete

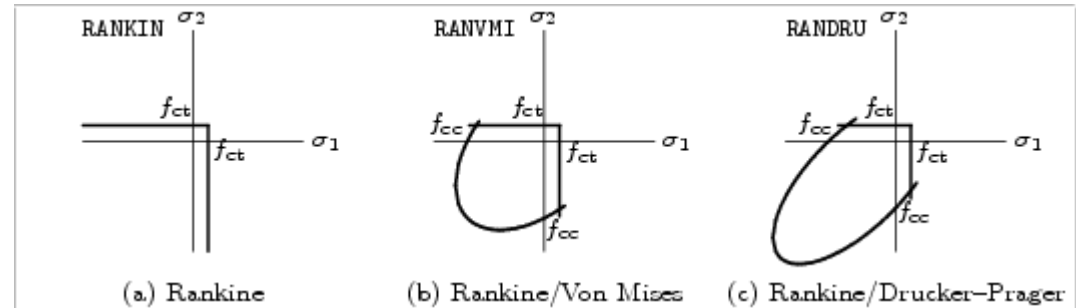
Ansys



(Viewed along the hydrostatic pressure axis)

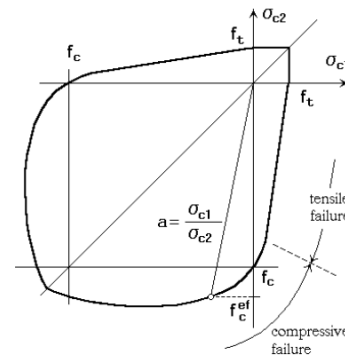


Diana

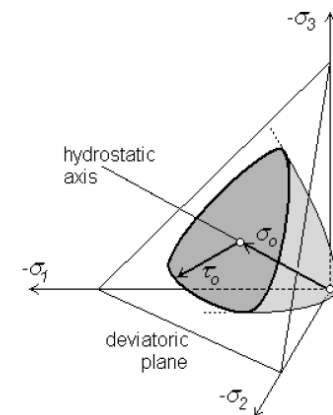


Atena

Bi-axial criterion



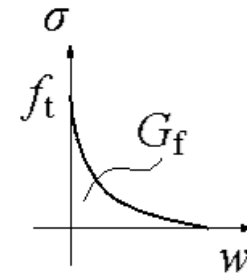
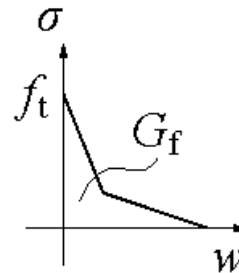
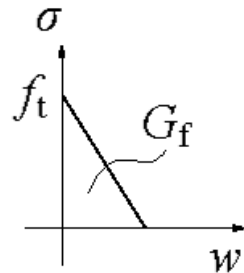
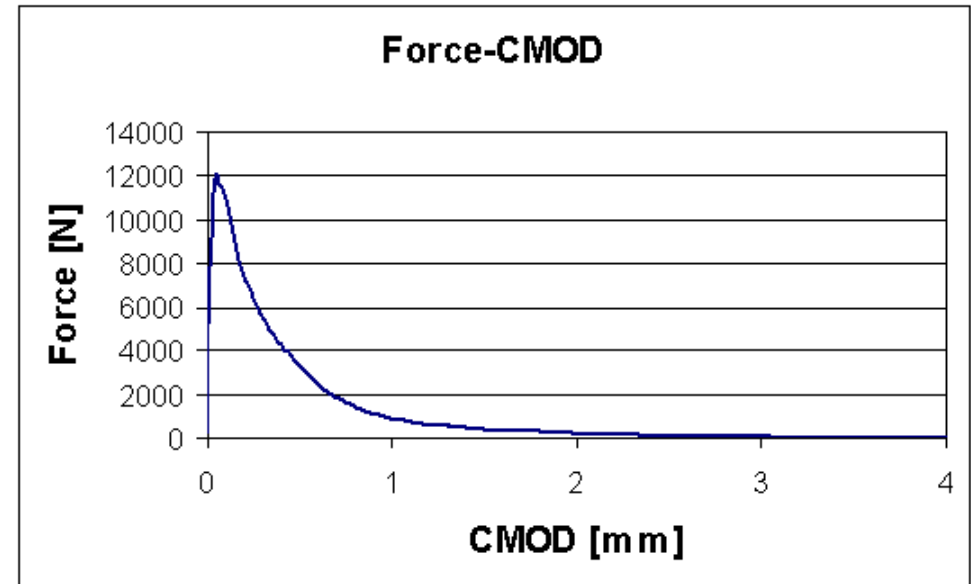
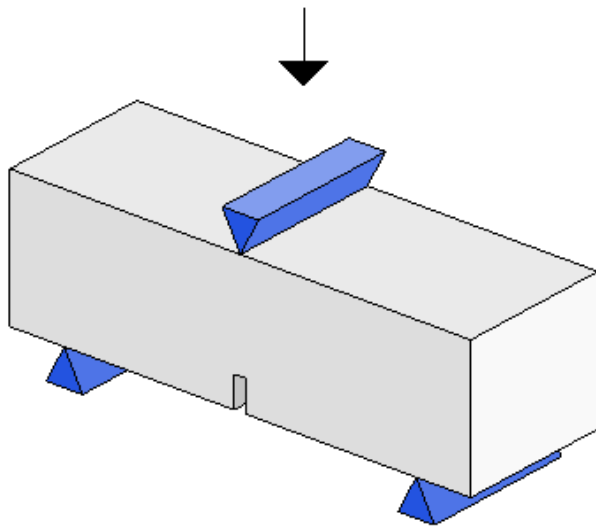
Kupfer 1969



Menetrey Willam, ACI 1995

B1. Material models from linear elastic to concrete

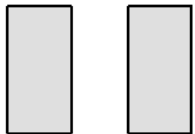
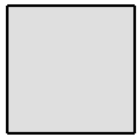
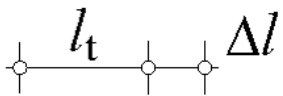
2) Quasi-brittle after crack



B1. Material models

from linear elastic to concrete

3) Localized cracks – $\sigma(w)$ instead of $\sigma(\varepsilon)$ – crack band size model



$$w = \Delta l (l_t)$$

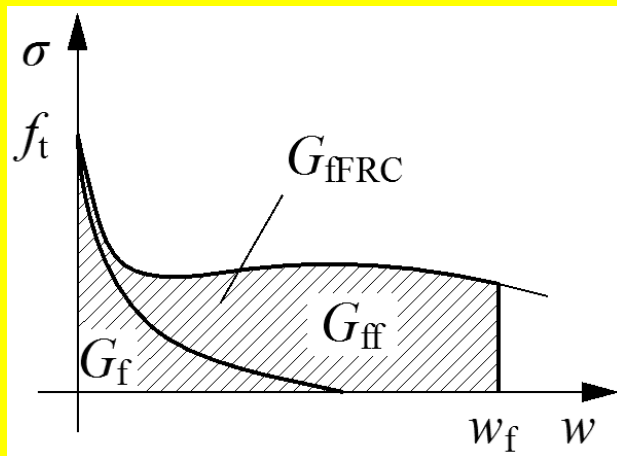
σ - w diagram \rightarrow σ - ε diagram

depends on the element size!
need **characteristic length**, l_{cs}

Bernoulli-Navier hypothesis is not valid

In summary, the material model used for modelling FRC must include the following:

- A combined failure surface for modelling of peak strength,
- Inclusion of the fracture energy (G_f) parameter for modelling of post-cracking performance,
- The fracture energy can be determined from the back analysis of test results.
- A stress-strain model that incorporates crack band theory to resolve the mesh dependency issue.

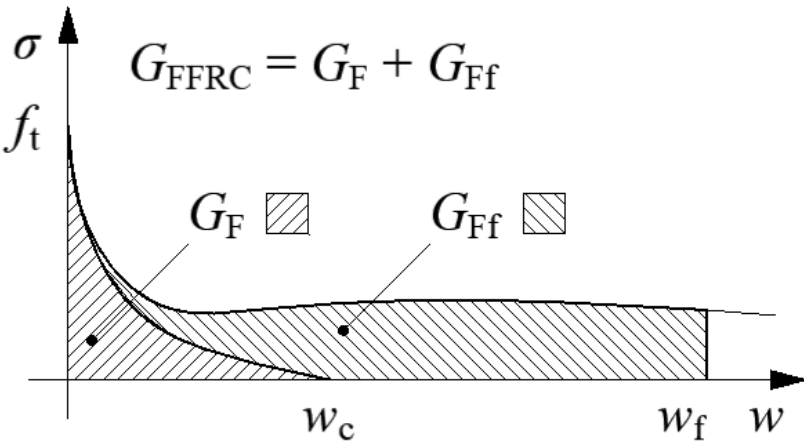


Modified Fracture Energy Method (MFEM) for fiber reinforced concrete (Juhasz, 2013).

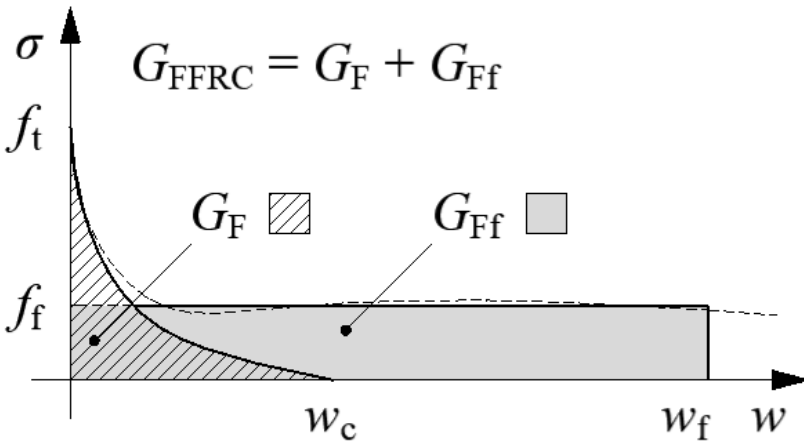
Fracture energy of FRC consists of fracture energy of the concrete (G_f) and added fracture energy of the fiber (G_{ff}).

A simplified constitutive law derived from test results will be used in Atena as a material model.

B2. Added Fracture Energy – FibreLAB

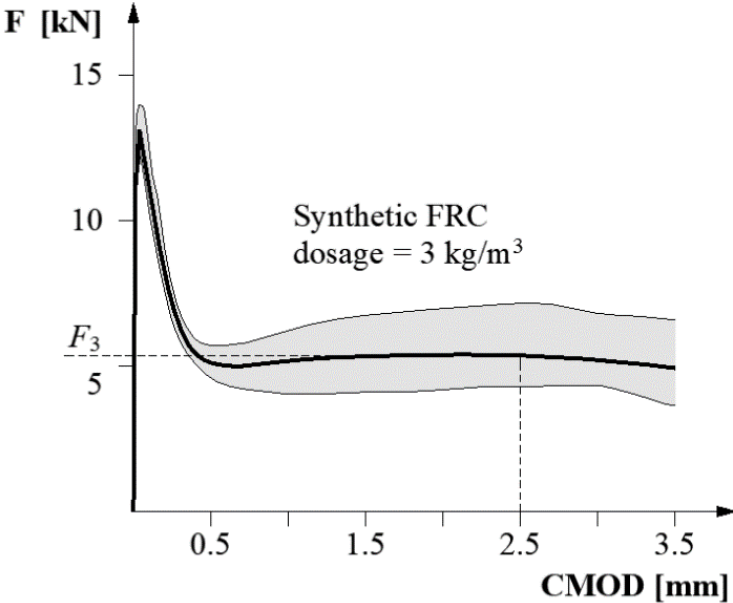


experimental diagram

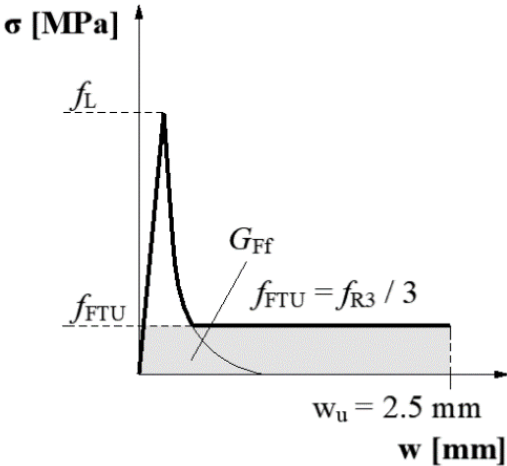


numerical diagram

Load-CMOD diagrams



Material model for ULS



B2. Added Fracture Energy – FibreLAB



Verification of the ATENA material model can be found on our homepage: **www.jkpstatic.com/FEA**

Toronto Shear Test

Shanghai Metro Tunnel Extension

PCAT Precast Tramline Project

Blind Simulation Competition (BSC) on Punching Shear

Debrecen Stadium Grandstand Modeling

Manholes exposed to railway loads

C. Applications and case studies

C1. Jointless floors and their challenges

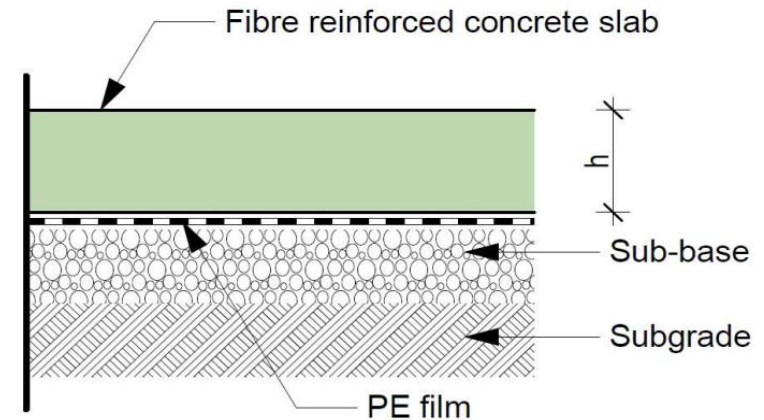
Slab on grade: PC/FRC/RC/HYB slab structure supported on lower surface

Concrete have shrinkage → stress → cracks
→ need of dilatation

No standard/guideline cover the design of the length of dilatation

Increased importance of carbon footprint → macro synthetic fiber reinforced concrete

Dilatations of 5-6 m → 20-25-30 m: called jointless, no saw-cut joints



C1. Jointless floors and their challenges

Loads:

- point (loads of shelf legs, and vehicle wheels),
- linear (loads imposed by walls or rails),
- surface (materials stored on a surface, where large supports are treated as surface loads).

Effects: temperature and shrinkage

- the friction prevents free movement, leading to tensile stresses
- the amount of stress depends primarily on the geometry of the floor, magnitude of friction
- the temperature effects can occur within a daily timeframe

Stresses caused by external forces should be combined by internal effects.

The actual load bearing capacity may be lower than if only external loads are considered.

C2. Cracks – our enemy : shrinkage

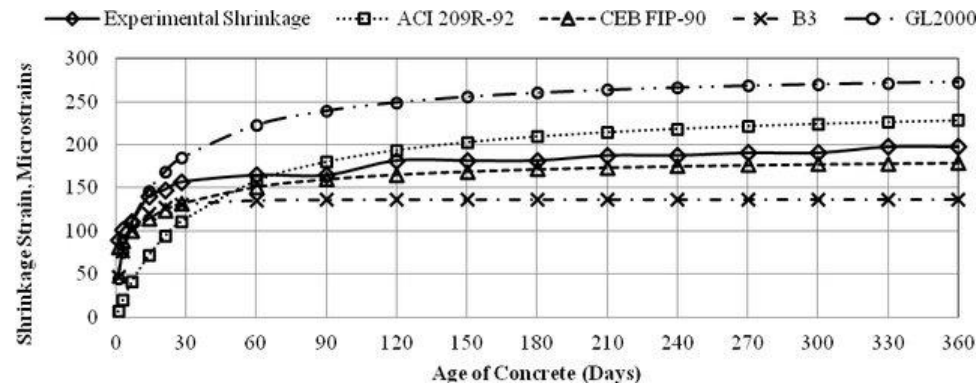
Concrete shrinks after hardening

The shrinkage is measured in $\mu\text{m}/\text{m}$

Many standardized method to measure, we can use **ASTM C157**

Many analytical model exist, we use **EUROCODE** model

Two basic type of shrinkage: autogenous and drying shrinkage



Designation: C 157/C 157M – 08

Standard Test Method for
Length Change of Hardened Hydraulic-Cement Mortar and
Concrete¹

C2. Cracks – our enemy : shrinkage

Effect of shrinkage is calculated by Eurocode 2 as below

Main parameters:

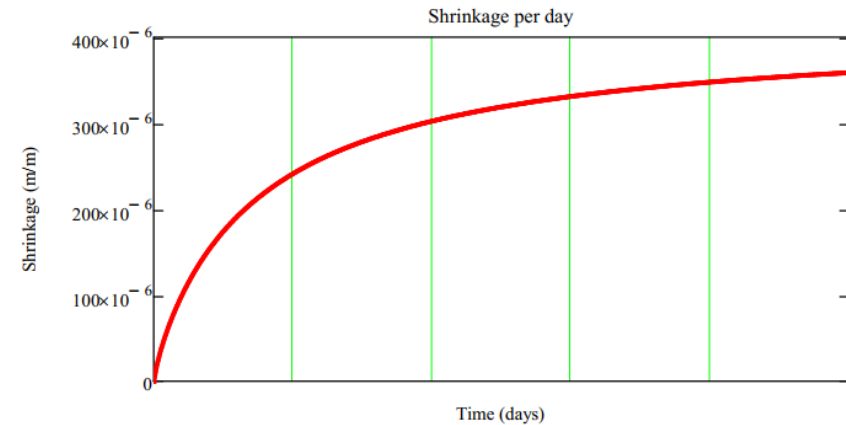
- Thickness
- Concrete strength
- Cement type
- Relative humidity

$$\varepsilon_{cd}(t) := \min(\beta_{ds}(t) \cdot k_h \cdot \varepsilon_{cd,0}, \varepsilon_{cd,max}) \quad \text{drying shrinkage}$$

$$\varepsilon_{ca} := 2.5 \cdot \left(\frac{f_{ck}}{\text{MPa}} - 10 \right) \cdot 10^{-6} = 37.5 \cdot \frac{\mu\text{m}}{\text{m}}$$

$$\varepsilon_{ca}(t) := \beta_{as}(t) \cdot \varepsilon_{ca} \quad \text{autogenous shrinkage}$$

$$\varepsilon_{cs,EC}(t) := \varepsilon_{cd}(t) + \varepsilon_{ca}(t)$$



green vertical line: 1 year

$$\varepsilon_{cs,EC}(365) = 241 \cdot \frac{\mu\text{m}}{\text{m}}$$

$$\varepsilon_{cs,EC}(2 \cdot 365) = 302 \cdot \frac{\mu\text{m}}{\text{m}}$$

$$\varepsilon_{cs,EC}(3 \cdot 365) = 331 \cdot \frac{\mu\text{m}}{\text{m}}$$

$$\varepsilon_{cs,EC}(5 \cdot 365) = 359 \cdot \frac{\mu\text{m}}{\text{m}}$$

C2. Cracks – our enemy : shrinkage

Shrinkage can be calculated by determining the moisture content of the concrete.

There is an approximately linear correlation between concrete shrinkage and moisture loss:

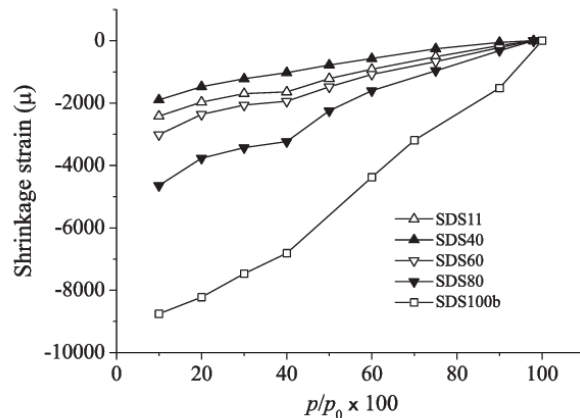


Fig. 24. Short term length change isotherm (SLCI) at 20 °C of the samples SDS100b, 80, 60, 40, and 11. SDS100b is the sample before drying, and SDS80–SDS11 were the samples dried for 12 months.

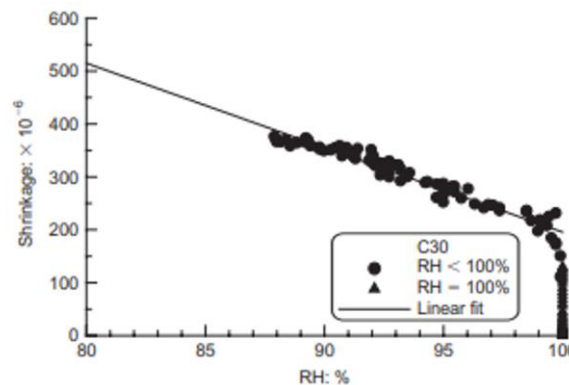


Figure 7. Relationship between free shrinkage strain and interior RH of C30 concrete

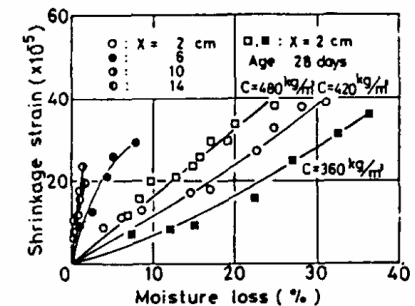


FIG. 13

The relationships between drying shrinkage strain and moisture losses

Maruyama, I., Nishioka, Y., Igarashi, G., & Matsui, K. (2014). Microstructural and bulk property changes in hardened cement paste during the first drying process. *Cement and Concrete Research*, 58, 20-34.

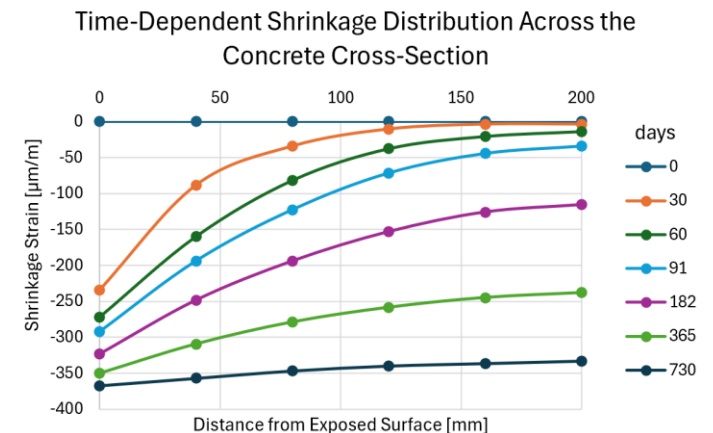
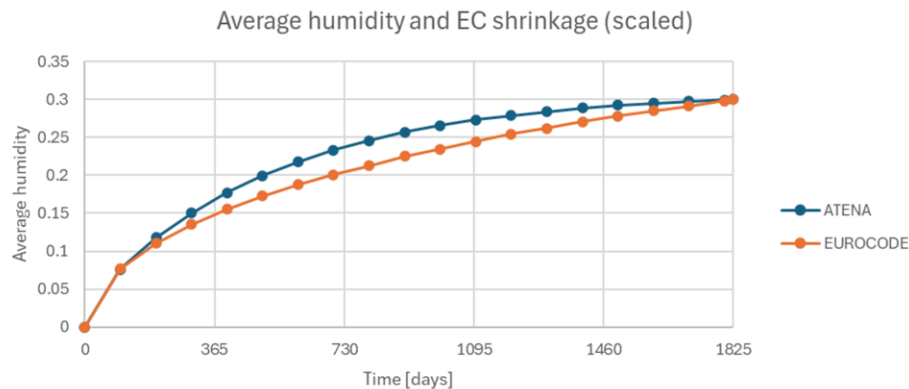
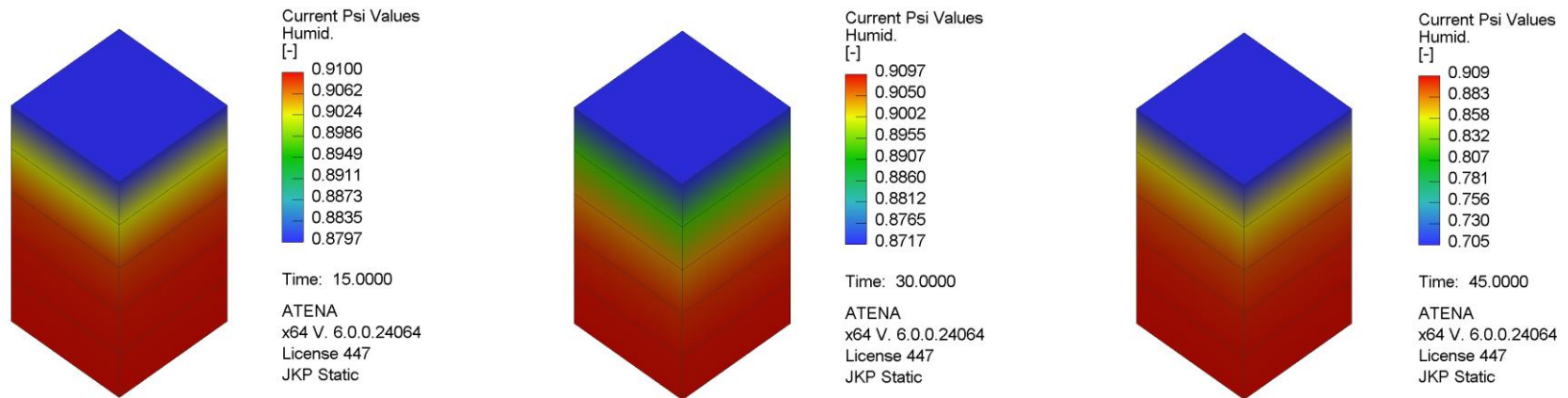
Zhang, J., Dongwei, H., & Wei, S. (2010). Experimental study on the relationship between shrinkage and interior humidity of concrete at early age. *Magazine of Concrete Research*, 62(3), 191-199.

Sakata, K. (1983). A study on moisture diffusion in drying and drying shrinkage of concrete. *Cement and Concrete Research*, 13(2), 216-224.

C2. Cracks – our enemy : shrinkage

Shrinkage can be calculated by determining the moisture content of the concrete.

There is an approximately linear correlation between concrete shrinkage and moisture loss:

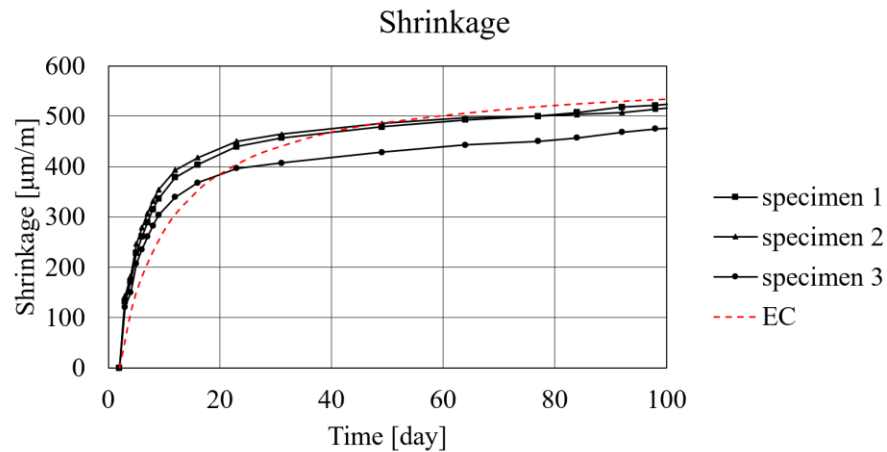


C2. Cracks – our enemy : shrinkage

How we measure?

Black: what we have measured

Red: EUROCODE analytical model



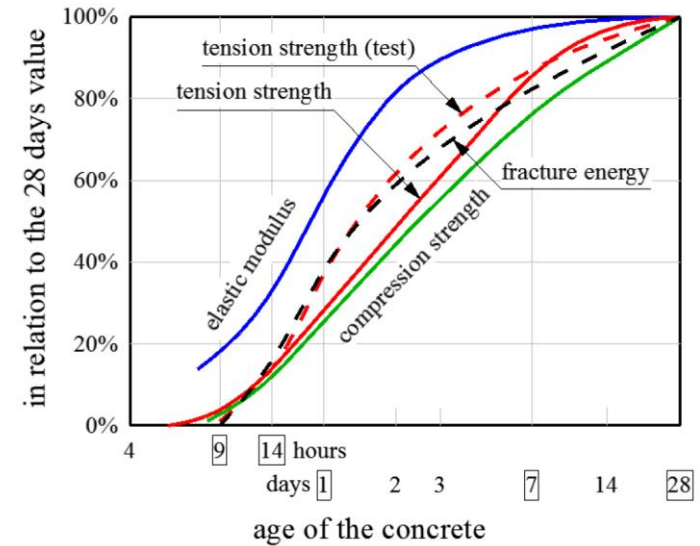
C3. Cracks – our enemy : early age cracks

Concrete strength increase during hardening
– but this increase is not linear (see diagram)

However, shrinkage is at its highest increase during early age period

So, increased attention should be paid at early age to prevent the development of cracks

Can fiber help here?



Juhász KP, Schaul P (2015) Modelling of early age shrinkage cracks with steel or synthetic macro fibre reinforcement in jointless floors, in: FIBRE CONCRETE 2015

C3. Cracks – our enemy : early age cracks

Shrinkage ring test according to Richtlinie Faserbeton (Austrian guideline)



0: plain concrete

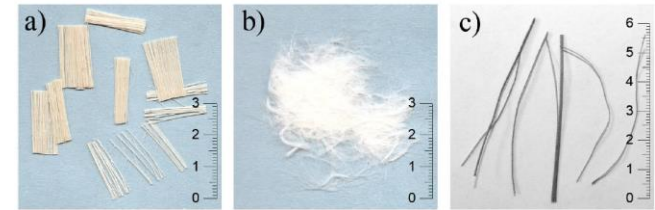
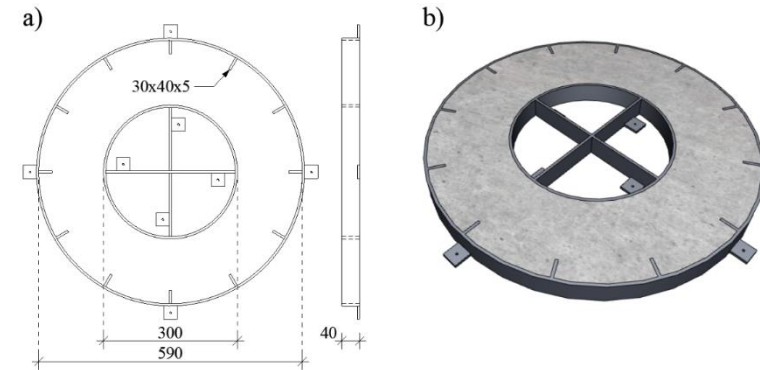
M1: fibrillated fiber (High Grade)

M2: monofilament (PP)

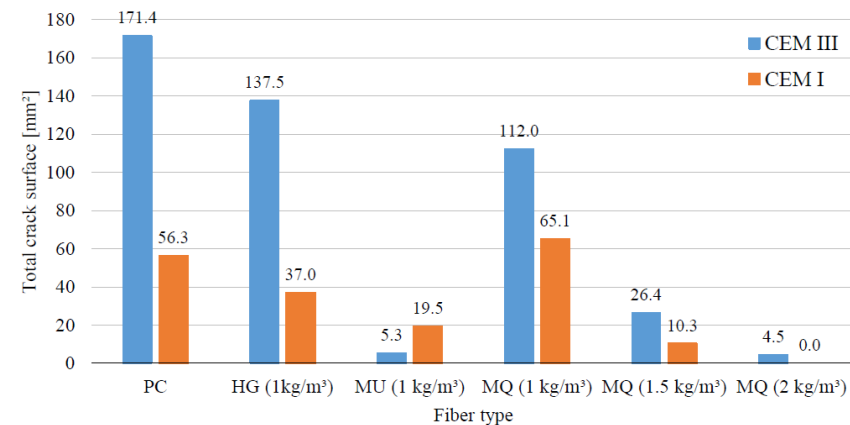
M3: BarChip MQ58 with 1 – 1.5 – 2.0 kg/m³ dosages

Even at 1.5 kg/m³ dosage we have a huge effect!

So MQ helps at early age cracks.



Total crack surface



C3. Cracks – our enemy : crack localization

Difference between tension softening and tension hardening FRC.

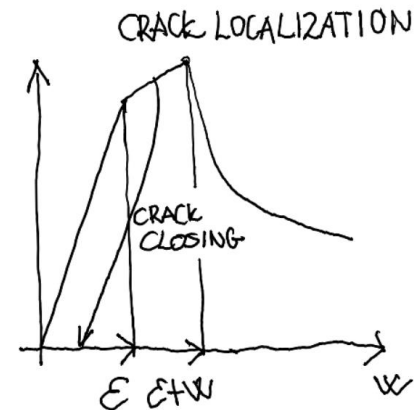
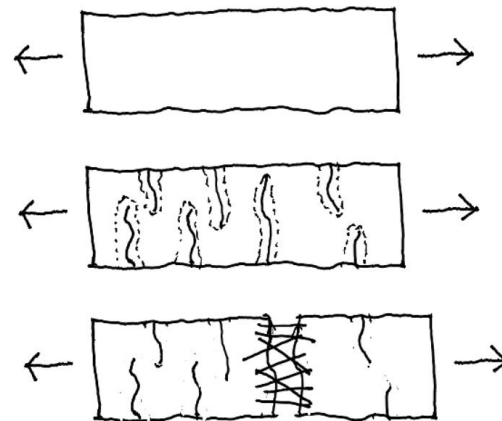
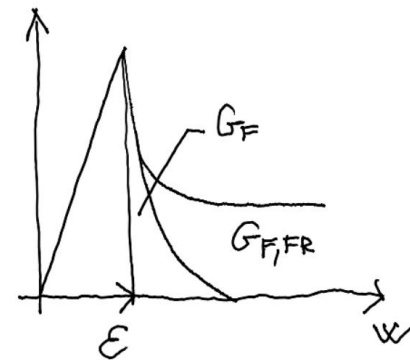
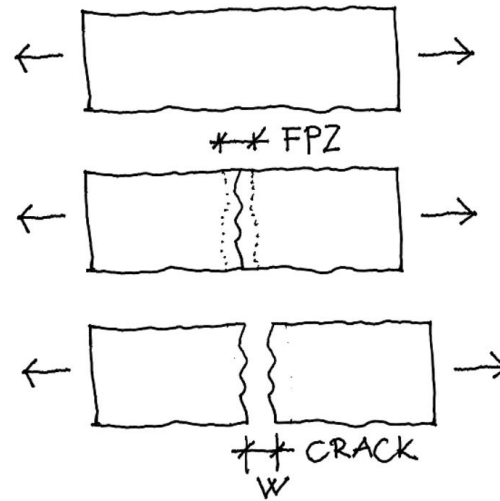
Synthetic FRC is always tension softening.

So, after the appearance of the first crack the other micro crack closing and only this first and only crack will open.

Leading to one, big crack.

On the contrary, tension hardening material have multiply cracks.

Can we use tension softening for preventing crack localization?

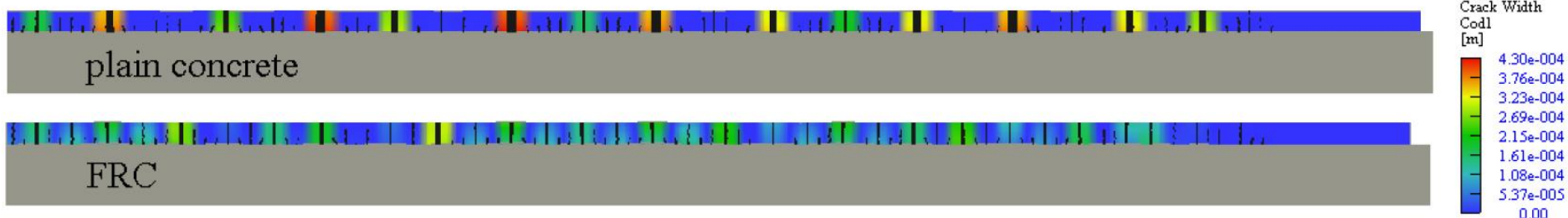
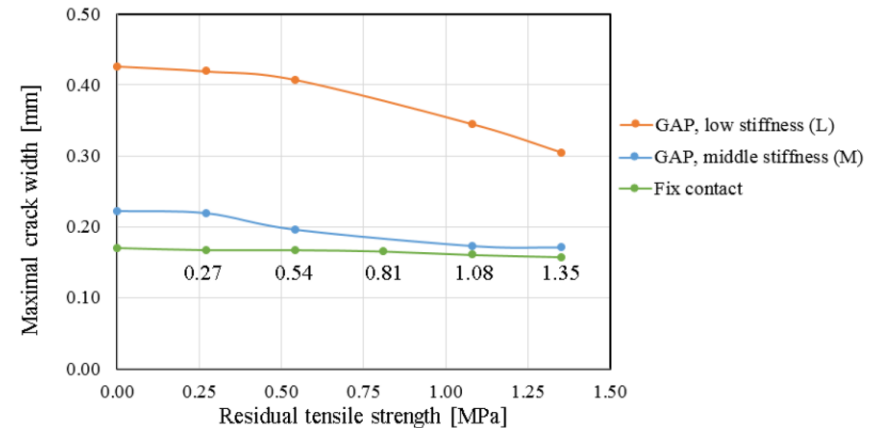


C3. Cracks – our enemy : crack localization

First research to understand the basic effects of FRC in 2015 – industrial floor in 2D.

Increasing residual tensile strength will decrease the maximum crack width – however, increasing the friction decrease the maximum crack width also.

So, residual strength and friction works together to eliminate crack localization.



Juhász KP, Schaul P (2015) Modelling of early age shrinkage cracks with steel or synthetic macro fibre reinforcement in jointless floors, in: FIBRE CONCRETE 2015

C3. Cracks – our enemy : crack localization

About the friction: how big?

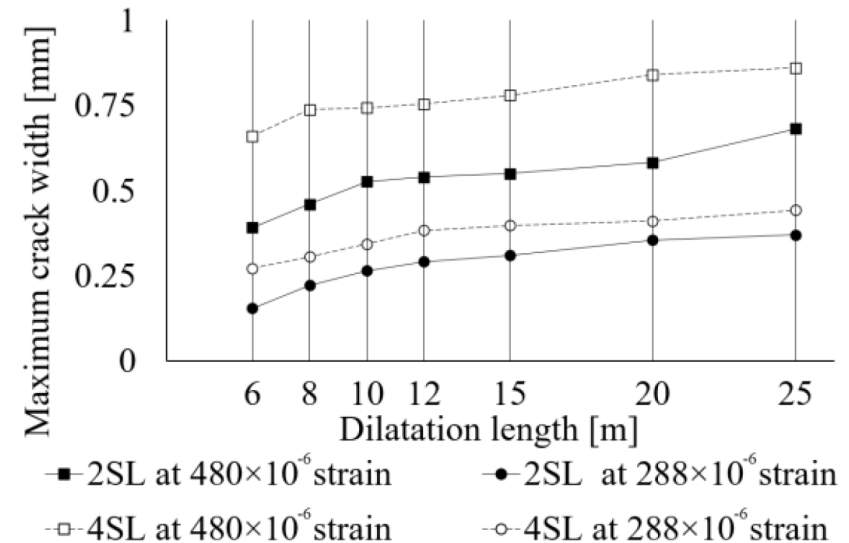
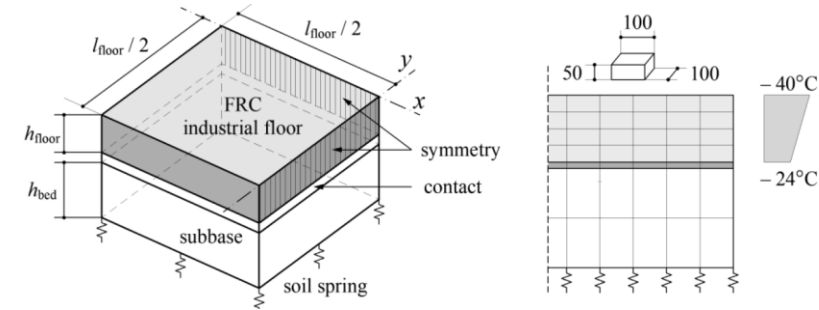
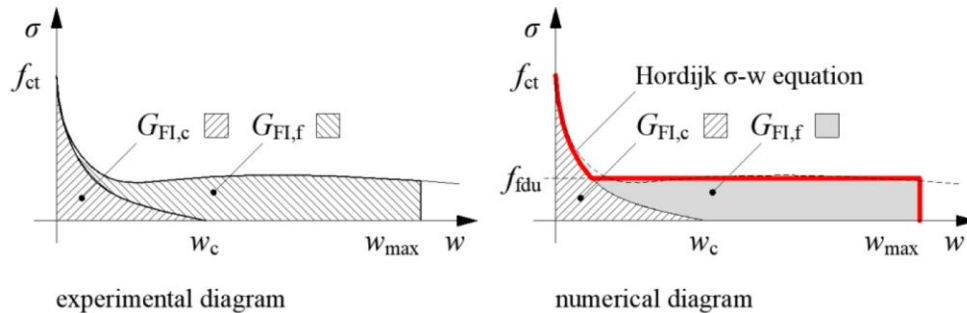


C3. Cracks – our enemy : crack localization

Research continued in 2023 – ATENA numerical models in 3D.

Maximum crack width increases with increase of the dilatation length, but with less intensity.

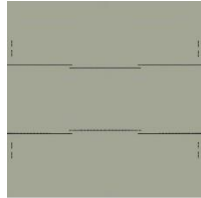
The reason is the floor dilatates itself with the cracks.



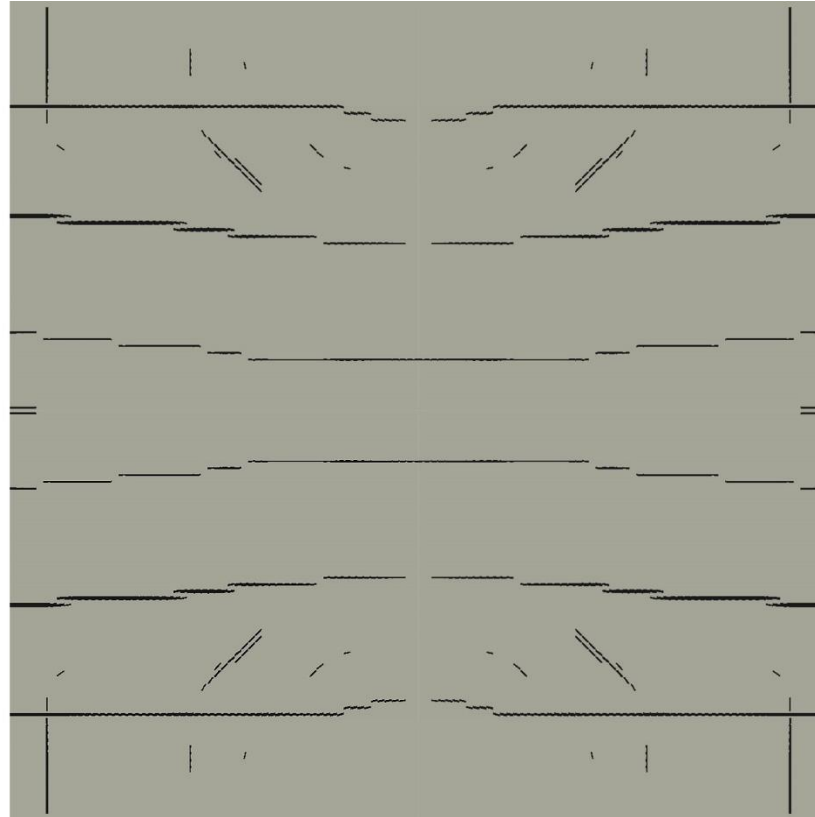
Juhász KP, Schaul P (2023) Parametric numerical study on jointless macro synthetic fiber reinforced concrete industrial floors, Joint ACI-fib-RILEM International Workshop

C3. Cracks – our enemy : crack localization

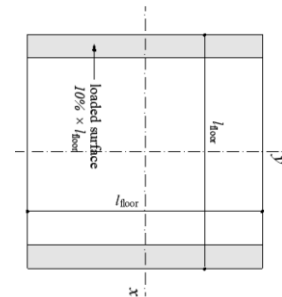
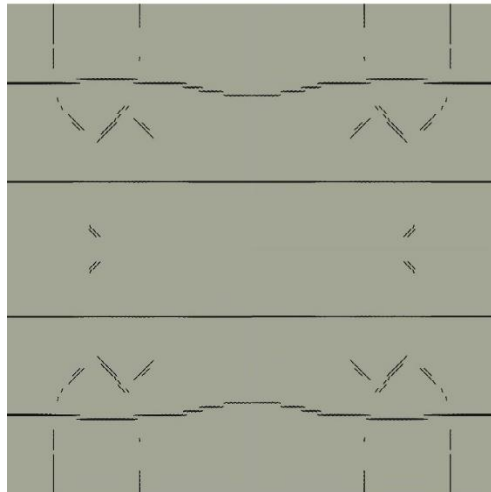
6m



25 m

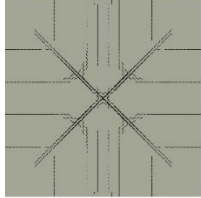


15 m

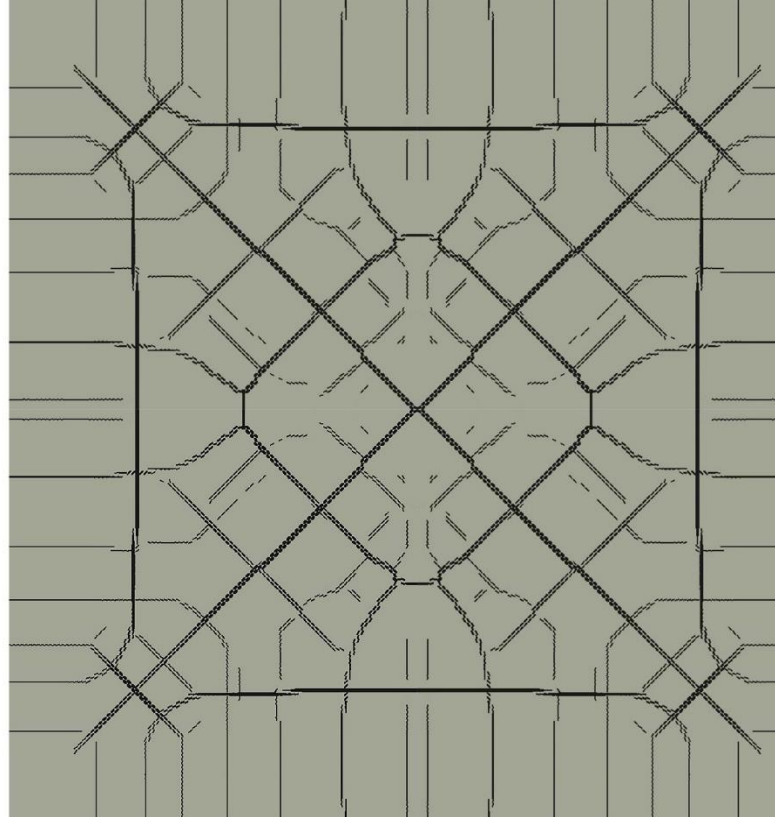


C3. Cracks – our enemy : crack localization

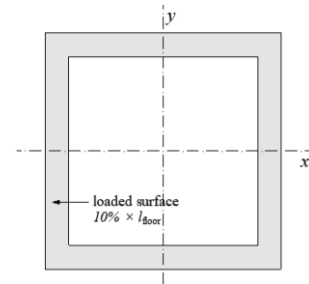
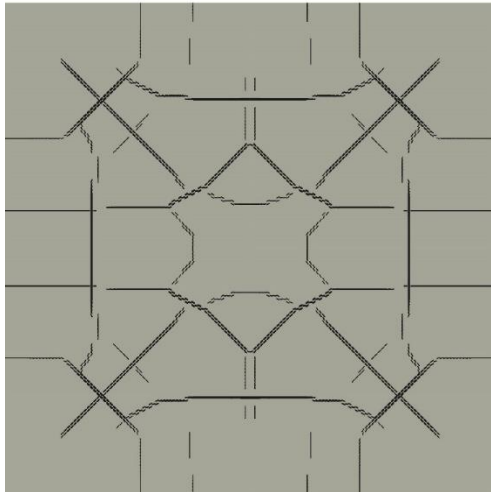
6m



25 m



15 m

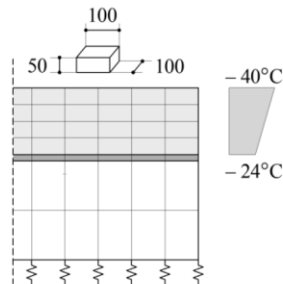
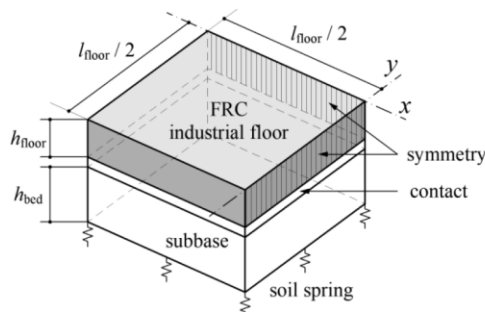


C4. Case study: HelloParks

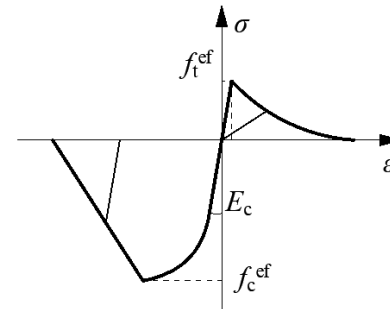
ATENA finite element software was used for modelling

The effect of the fibres was defined according to **fib** Model Code 2010 and modelled with the Modified Fracture Energy Method

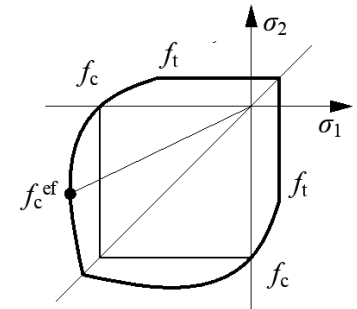
Shrinkage effect was calculated according to Eurocode



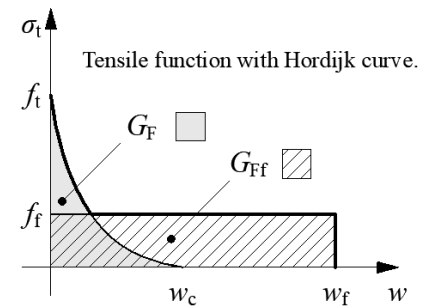
Stress-strain Law



Biaxial Failure Law

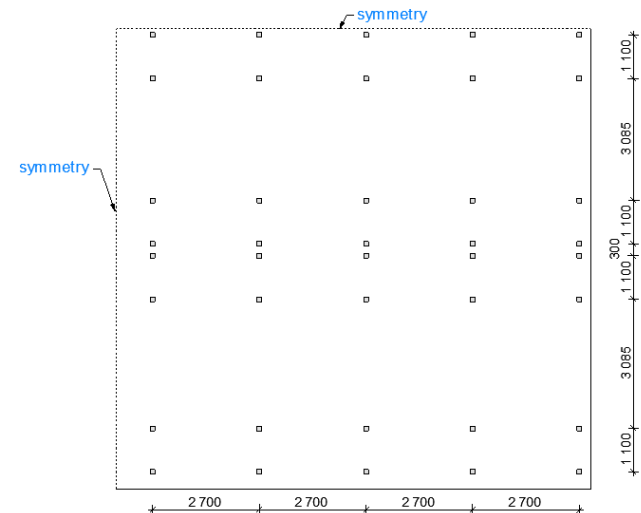
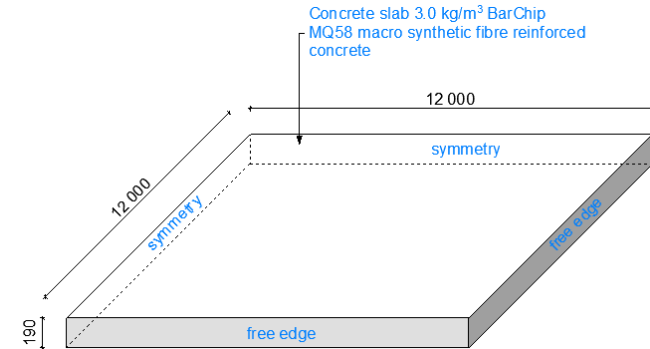


Tension Function



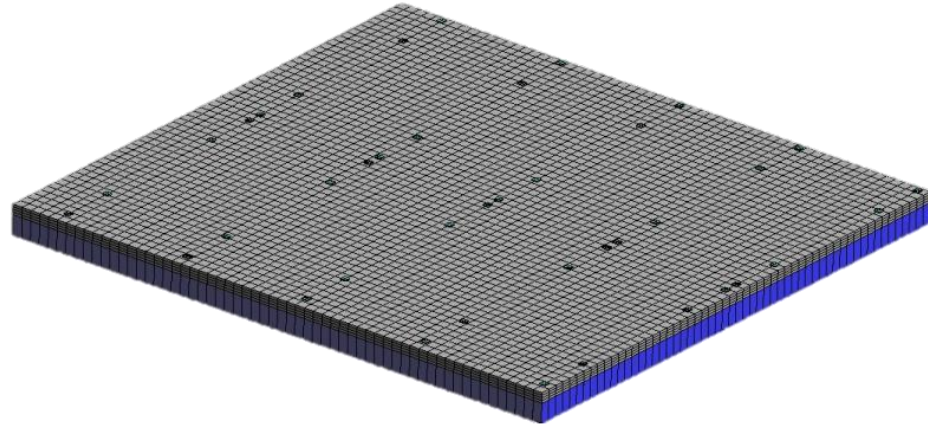
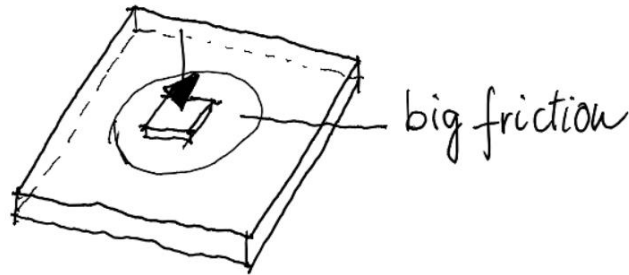
C4. Case study: HelloParks

- 100.000 m² industrial floor in Hungary
- 24 × 24 m joint distance
- 190 mm thickness
- C30/37 concrete
- Rack leg load characteristic value is 50 kN
- Crack width limit is 0.3 mm
- **Goal: find the optimum solution**



C4. Case study: HelloParks

- FEA was made with exact rack load positions → big friction under rack legs
- Shrinkage was calculated according to EC



$$t_s := 7$$

end of curing

$$f_{ck} := 30 \text{ MPa}$$

characteristic compressive strength

$$f_{cm} := f_{ck} + 8 \text{ MPa}$$

$$d := h = 210 \text{ mm}$$

thickness of the floor

$$l_d := 24 \text{ m}$$

dilatation length

$$u := l_d$$

perimeter of the drying cross section

$$A_c := d \cdot l_d = 5.04 \text{ m}^2$$

cross section

$$h_0 := \frac{2 \cdot A_c}{u} = 420 \text{ mm}$$

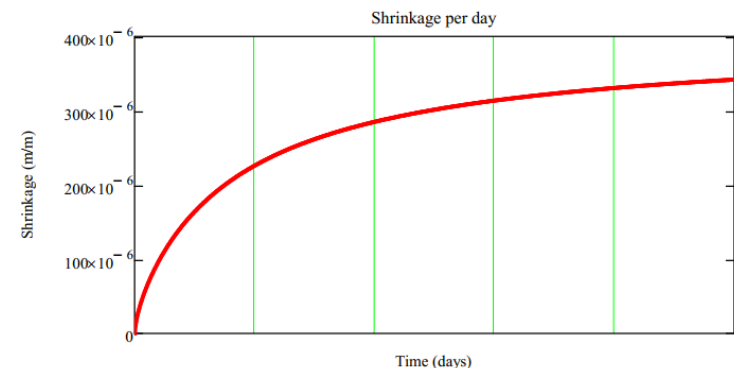
notional size of the cross section

$$\epsilon_{cs,EC}(365) = 226 \cdot \frac{\mu\text{m}}{\text{m}}$$

$$\epsilon_{cs,EC}(2 \cdot 365) = 285 \cdot \frac{\mu\text{m}}{\text{m}}$$

$$\epsilon_{cs,EC}(3 \cdot 365) = 314 \cdot \frac{\mu\text{m}}{\text{m}}$$

$$\epsilon_{cs,EC}(5 \cdot 365) = 342 \cdot \frac{\mu\text{m}}{\text{m}}$$

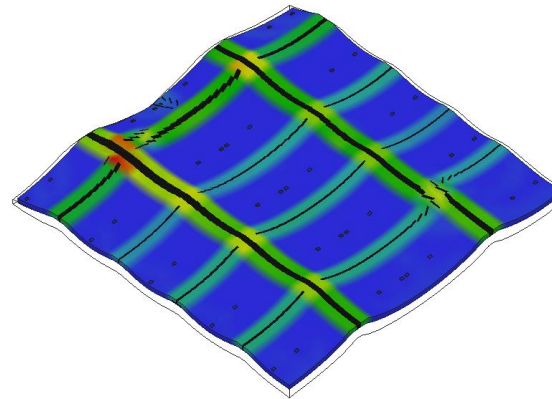


C4. Case study: HelloParks

76 kN load

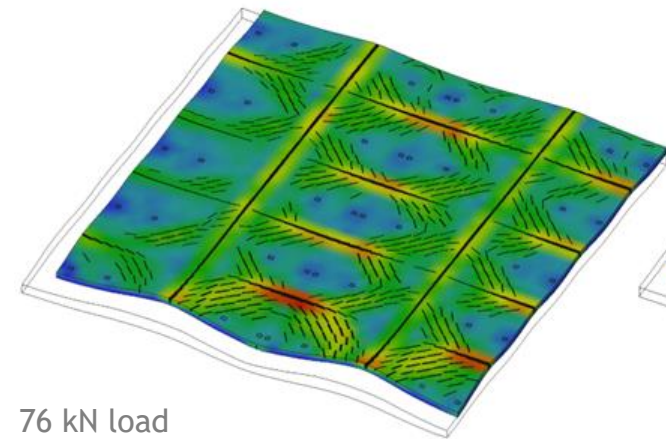
Plain concrete solution

$w_{\max} : 1.49 \text{ mm}$



Crack Width
Cod1
[m]
0.00149
0.00131
0.00112
0.00093
0.00075
0.00056
0.00037
0.00019
0.00000

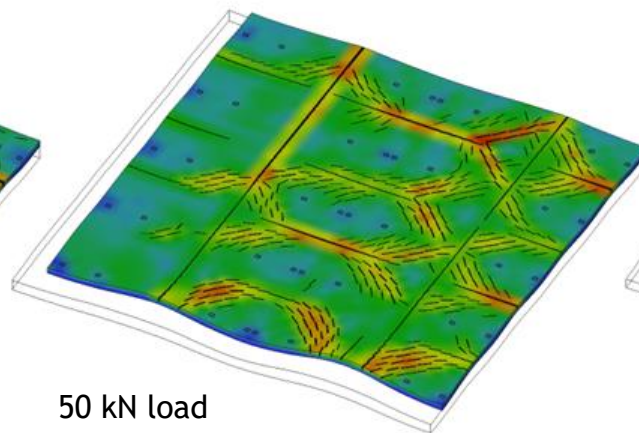
Deformation scale:
300.8654252
Time: 253.000
ATENA
x64 V. 5.9.1.21517
License 447
JKP Static



76 kN load

3 kg/m³ BarChip MQ58 fibre dosage

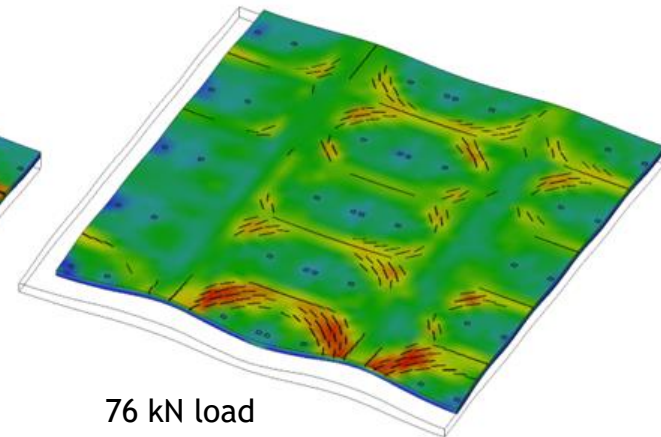
$w_{\max} : 0.269 \text{ mm}$



50 kN load

3 kg/m³ BarChip MQ58 fibre dosage

$w_{\max} : 0.202 \text{ mm}$



76 kN load

5 kg/m³ BarChip MQ58 fibre dosage

$w_{\max} : 0.158 \text{ mm}$

C4. Case study: HelloParks

Final solution was with 3 kg/m³ BarChip MQ58 fibre dosage

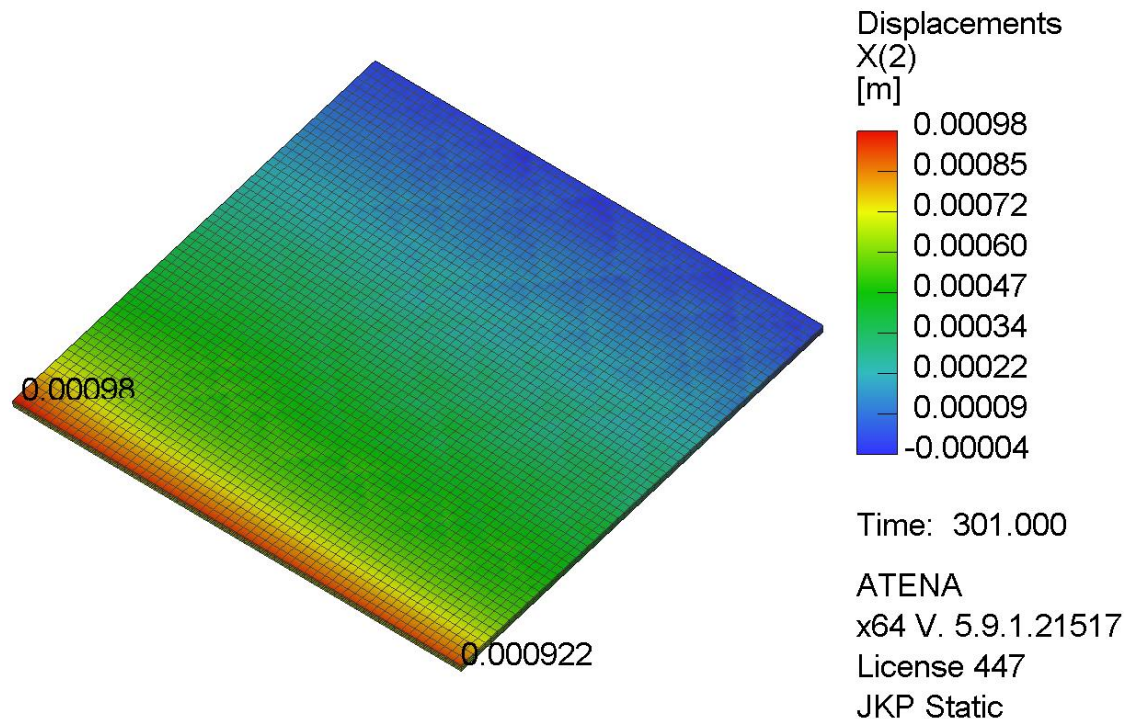
The construction started at 08.09.2023



C5. Future research

1) Verification on an Industrial Floor

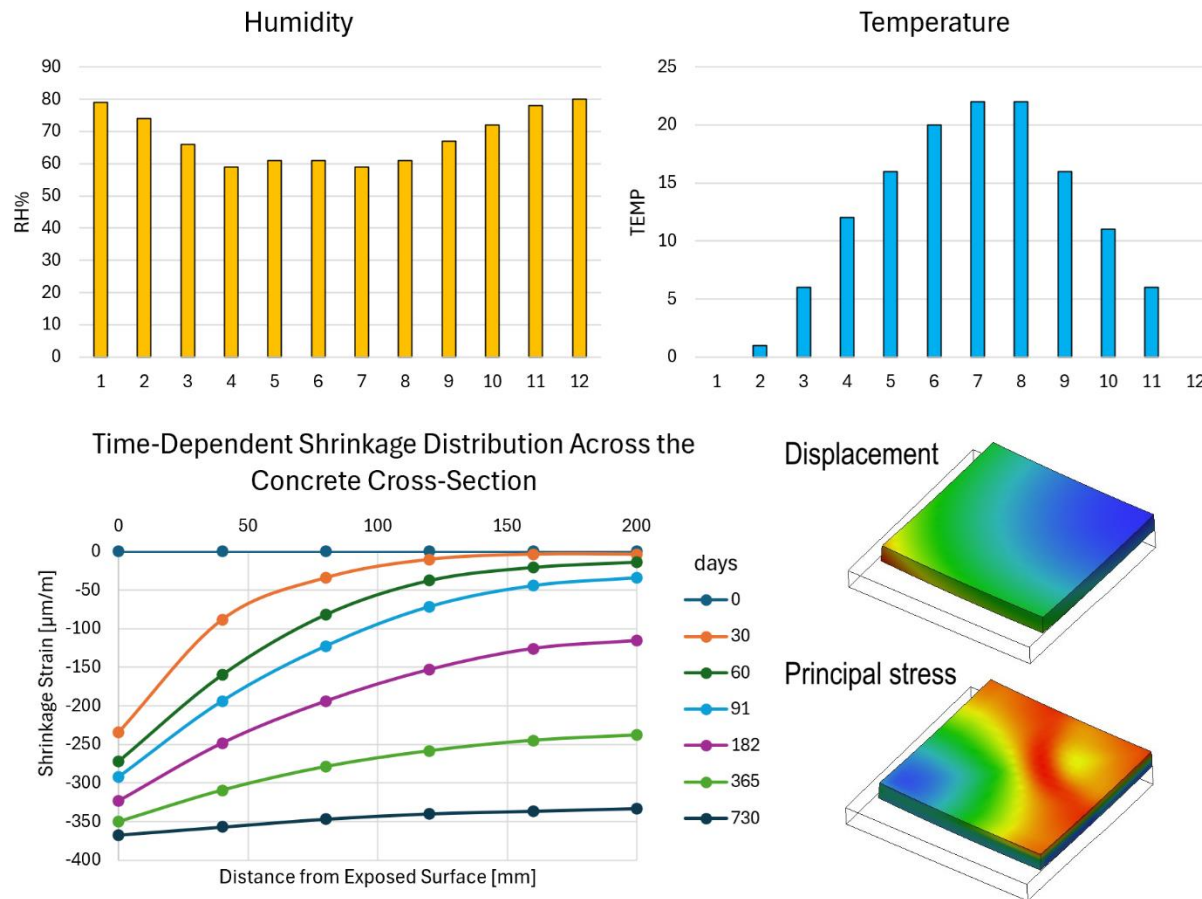
We are conducting research to validate our analytical model. Weekly measurements of horizontal displacements at the columns are compared with model predictions. The approach allows us to simulate dilatation profiles, reinforcement, and to analyze the role of floor–subbase friction.



C5. Future research

2) Time-Dependent Humidity and Temperature Changes – A New Approach to Modeling Outdoor Pavements

We propose a novel modeling framework that incorporates time-varying humidity and temperature effects. This enables more realistic prediction of pavement behavior under outdoor environmental conditions.



Thank you for your attention!



www.jkpstatic.com

www.linkedin.com/company/jkp-static